

Results from The COPAINS Pilot Survey: four new brown dwarfs and a high companion detection rate for accelerating stars

M. Bonavita^{1,2,3*}, C. Fontanive⁴, R. Gratton³, K. Mužić⁵, S. Desidera³, D. Mesa³, B. Biller², A. Scholz⁶, A. Sozzetti⁷, V. Squicciarini^{3,8}

¹*School of Physical Sciences, The Open University, Walton Hall, Milton Keynes, MK7 6AA*

²*SUPA, Institute for Astronomy, University of Edinburgh, Blackford Hill, Edinburgh EH9 3HJ, UK*

³*INAF Osservatorio Astronomico di Padova, Vicolo dell'Osservatorio 5, 35121 Padova, ITALY*

⁴*Center for Space and Habitability, University of Bern, Bern 3012, Switzerland*

⁵*CENTRA, Faculdade de Ciências, Universidade de Lisboa, Ed. C8, Campo Grande, P-1749-016 Lisboa, Portugal*

⁶*SUPA, School of Physics & Astronomy, University of St Andrews, North Haugh, St Andrews, KY16 9SS, UK*

⁷*INAF - Osservatorio Astrofisico di Torino, Via Osservatorio 20, 10025, Pino Torinese, Italy*

⁸*Department of Physics and Astronomy Galileo Galilei, University of Padova, Via dell'Osservatorio 3, I-35122 Padova, Italy*

Accepted 2022 April 25. Received 2022 April 21; in original form 2022 April 08

ABSTRACT

The last decade of direct imaging (DI) searches for sub-stellar companions has uncovered a widely diverse sample that challenges the current formation models, while highlighting the intrinsically low occurrence rate of wide companions, especially at the lower end of the mass distribution. These results clearly show how blind surveys, crucial to constrain the underlying planet and sub-stellar companion population, are not an efficient way to increase the sample of DI companions. It is therefore becoming clear that efficient target selection methods are essential to ensure a larger number of detections. We present the results of the COPAINS Survey conducted with SPHERE/VLT, searching for sub-stellar companions to stars showing significant proper motion differences ($\Delta\mu$) between different astrometric catalogues. We observed twenty-five stars and detected ten companions, including four new brown dwarfs: HIP 21152 B, HIP 29724 B, HD 60584 B and HIP 63734 B. Our results clearly demonstrates how astrometric signatures, in the past only giving access to stellar companions, can now thanks to Gaia reveal companions well in the sub-stellar regime. We also introduce FORECAST (Finely Optimised REtrieval of Companions of Accelerating STars), a tool which allows to check the agreement between position and mass of the detected companions with the measured $\Delta\mu$. Given the agreement between the values of the masses of the new sub-stellar companions from the photometry with the model-independent ones obtained with FORECAST, the results of COPAINS represent a significant increase of the number of potential benchmarks for brown dwarf and planet formation and evolution theories.

Key words: stars: brown dwarfs, stars: low mass, (stars) binaries: visual, instrumentation: adaptive optics, astrometry

1 INTRODUCTION

Direct imaging (DI) is the only detection method that provides observations of an exoplanet or brown dwarf (BD) itself, as it captures the thermal emission of self-luminous companions. With the unique opportunity to obtain photometric and spectroscopic observations of substellar objects, this detection method allows for a direct probe of cold companions atmospheres. DI is also necessary to study the outer regions of planetary systems, that cannot be probed by other detection methods.

Despite the remarkable efforts that have been invested in the development of new observing technologies and image processing techniques, and a steady increase in the census of wide-orbit companions, only a handful of systems below the deuterium-burning limit have been uncovered around stars in DI programs, and the occurrences of wide companions appear to be intrinsically low (Biller et al. 2007,

2013; Lafrenière et al. 2007; Nielsen & Close 2010; Vigan et al. 2012, 2017, 2021; Rameau et al. 2013; Galicher et al. 2016a; Nielsen et al. 2019). In order to empirically constrain the formation, evolution, and atmospheric properties of both isolated and bound sub-stellar companions, we need to uncover a substantial population of these objects, and measure their fundamental properties, such as the effective temperature and mass. However, even when a comprehensive view and an extensive spectro-photometric characterisation is possible, imaging surveys still only provide measurements of an object's luminosity. Mass estimates for imaged planets and brown dwarfs therefore rely entirely on evolutionary models, which currently carry high uncertainties, particularly at young to intermediate ages. An independent determination of masses from dynamical arguments is therefore crucial to overcome the large uncertainties introduced by evolutionary models, and in turn refine the theories. Furthermore, a sample of benchmark objects should ideally span a wide range of properties (e.g., spectral types, masses, ages). As direct imaging is more amenable to very young systems, where low-mass companions

* E-mail: mariangela.bonavita@open.ac.uk

are still bright, the majority of the scarce sample of such benchmark objects in the planetary regime orbit relatively young stars (few tens to hundred Myr). On the contrary, most brown dwarf companions with well-defined dynamical masses orbit older hosts with field ages of several Gyrs (see Fig. 1). As known bound sub-stellar companions are even rarer in associations such as Hyades (~ 650 Myr [Martín et al. 2018](#)), the intermediate age regime remains relatively unexplored, and theoretical models are hence particularly poorly constrained at these ages. Our understanding of the origins and atmospheres of these objects thus remains severely limited by the small number of known systems. In particular, the sparse sample of directly-imaged companions show a large diversity of spectro-photometric characteristics and orbital configurations, and remain challenging to grasp as populations ([Bowler 2016](#)). Larger numbers of detections are hence essential to enable a better characterisation and understanding of the wide-orbit companion population, and obtain a clearer picture of their formation patterns.

In [Fontanive et al. \(2019\)](#), we presented a new tool COPAINS (Code for Orbital Parametrisation of Astrometrically Inferred New Systems), developed to identify previously undiscovered companions detectable via DI, based on changes in stellar proper motions across multiple astrometric catalogues. A significant proper motion difference ($\Delta\mu$) between two catalogues for a given star is a good indication of the presence of a perturbing body. For systems showing significant differences between proper motions measured over a long time baseline (e.g., Tycho-2, or Tycho *Gaia* Astrometric Solution - TGAS; [Høg et al. 2000](#); [Michalik et al. 2015](#)), and catalogues that provide short-term proper motions (e.g., Hipparcos, *Gaia* DR2; [ESA 1997](#); [Gaia Collaboration et al. 2018](#)), the tool allows for the computation of secondary mass and separation pairs compatible with the observed trend, marginalised over all possible orbital phases and eccentricities. The resulting solutions are based entirely on dynamical arguments, although a dependence on the adopted (usually model-derived) stellar mass remains in the obtained secondary masses. Compared to the expected sensitivity of an imaging instrument, these predictions can then be used to select the most promising targets for DI searches of low-mass companions.

The use of such informed selection processes had already proven to be effective in the stellar regime ([Makarov & Kaplan 2005](#); [Tokovinin et al. 2013](#); [Bowler et al. 2021](#); [Steiger et al. 2021](#)), and recently led to the discovery of new brown dwarf companions based on the astrometric signatures induced on their host stars ([Currie et al. 2020](#); [Chilcote et al. 2021](#)). Such astrometric systems are particularly valuable, as the combination of relative astrometry from DI information with absolute astrometry from the primary’s astrometric signature offers a remarkable opportunity to refine orbital constraints and measure dynamical masses ([Calissendorff & Janson 2018](#); [Snellen & Brown 2018](#); [Brandt et al. 2019](#); [Dupuy et al. 2019](#); [Grandjean et al. 2019](#); [Maire et al. 2020](#); [Nielsen et al. 2020](#); [Drimmel et al. 2021](#)). Precise orbital elements for the population of wide-orbit companions can provide key insights into formation mechanisms (e.g., [Bowler et al. 2020](#)). Furthermore, model-independent mass measurements for brown dwarfs and giant planets are especially important to bypass the use of mass estimates from theoretical models, which typically carry large uncertainties, both due to the difficulties of determining system ages, and to the systematic uncertainties of the evolutionary and atmosphere models which are particularly pronounced at the lowest masses and youngest ages. Increasing the pool of systems amenable to dynamical mass measurements will therefore be essential to help calibrate theoretical models for substellar objects.

In this paper, we present the results of a pilot survey conducted with the SPHERE instrument ([Beuzit et al. 2019](#)), an extreme adaptive

optics facility at the ESO’s Very Large Telescope (VLT), which employed the COPAINS tool for informed target selection. We describe the sample and selection method in Section 2. The observations and data reduction are presented in Section 3. The survey results are reported in Section 4 and discussed in Section 5.

2 SAMPLE PROPERTIES

2.1 Target Selection

2.1.1 Initial Target List

To select targets for DI campaigns, we searched different catalogues containing proper motions, using as an input a list of known, relatively young, sources, from which the targets protected by the SPHERE Guaranteed Time Observations (GTO) were removed. For the sources with both long- and short-term proper motion information, we first selected stars showing a difference larger than 3σ between two catalogues, in either of the proper motion components. The data presented here were obtained during three ESO periods (P100, P102, and P104)¹, with several differences in target selection procedure, as a result of the different *Gaia* data releases available at the time of each selection. The relevant information about the two initial selections are listed here.

Selection 1 (P100 and P102)

- Input list: An extensive compilation of about 900 nearby young stars ([Desidera et al. 2015](#)).
- Long-term proper motion catalogue: Tycho-2 ([Høg et al. 2000](#)), with a proper motion baseline of ~ 100 yr.
- Short-term proper motion catalogue: The Tycho-*Gaia* Astrometric Solution (TGAS; [Michalik et al. 2015](#)), part of *Gaia* DR1 ([Gaia Collaboration et al. 2016](#)), with a proper motion baseline of ~ 25 yr.

Selection 2 (P104)

- Input list: The same compilation as above ([Desidera et al. 2015](#)), complemented by bona-fide members of nearby young moving groups ([Gagné et al. 2018](#); [Gagné & Faherty 2018](#)). In total, there are about 2200 unique objects in this input list.
- Long-term proper motion catalogue: TGAS, with a proper motion baseline of ~ 25 yr.
- Short-term proper motion catalogue: *Gaia* DR2 ([Gaia Collaboration et al. 2018](#)), with a proper motion baseline of ~ 1.5 yr.

Following the selection of these so-called $\Delta\mu$ candidates, stars with known companions from visual and/or radial velocity observations were removed from the list. A star was removed if satisfying any of the following criteria:

- Multiplicity flag (MultiFlag) equal to C or O in the Hipparcos catalogue ([ESA 1997](#));
- Star appears in the Catalog of Components of Double & Multiple stars (CCDM; [Dommanget & Nys 2002](#));
- Star appears in The ninth catalogue of spectroscopic binary orbits (S_B^9 ; [Pourbaix et al. 2004](#));
- Star has a sub-stellar companion listed in The Extrasolar Planets Encyclopaedia²;

¹ ESO programme IDs 0100.C-0646, 0102.C-0506, 0104.C-0965

² <http://exoplanet.eu/>

- A suffix in the name of the star indicating that it is part of a binary system, or an unresolved binary (e.g. A, B, AB).
- For the Selection 2, we also excluded stars with another source closer than $5'$ on the sky, and sharing the same parallax (within 3σ), in order to exclude obvious stellar binaries from the survey and correctly focus on sub-stellar companions. For this, we only used the sources with a relatively small parallax uncertainties ($\varpi/\sigma_\varpi < 0.2$).

2.1.2 COPAINS Selection

After removing known binaries as detailed above, we further retained only the targets for which the COPAINS tool (Fontanive et al. 2019) returned that the objects causing the observed astrometric trends could be sub-stellar, if in the parameter space detectable with SPHERE (i.e., within the instrument field-of-view and above the expected sensitivity of observations).

COPAINS provides a good indication of the region of the parameter space in which a hidden companion responsible for an observed astrometric offset may be. Based on the formalism from Makarov & Kaplan (2005), the approach assumes that long-term proper motion measurements are representative of a system's centre-of-mass motion, and that short-term measurements correspond to the instantaneous reflex motion of the host star. For a measured $\Delta\mu$ value, the code allows us to evaluate the possible companion mass and separation pairs compatible with the astrometric data, for a given distance, stellar mass (see Section 2.3), and eccentricity distribution, while assuming face-on orbital inclinations (see Fontanive et al. 2019 for details). We adopted a Gaussian eccentricity distribution centred around $e=0$ with a width of 0.3 (Bonavita et al. 2013), and the astrometric catalogues listed above were used as long- and short-term proper motion values.

Figure 1 shows examples of the resulting trends computed with COPAINS for one target from P100 (left) and one target from P104 (right). In each case, the estimated solutions were compared to the expected sensitivity limit of SPHERE-IFS, shown as a red solid line in Figure 1. The IFS limits were obtained following the approach described by Mesa et al. (2021) and converted to minimum mass limits using the models from Baraffe et al. (2015) and the values of the age and stellar mass available at the time of the selection. Only promising targets, where the intersection of the detection limits and computed regions suggested possible sub-stellar companions detectable in our survey, were kept for the final sample, based on a visual analysis of the obtained plots. Finally, only the targets not previously observed with SPHERE, and observable in the relevant ESO period were kept. The final target list consisting of 25 stars observed with SPHERE is given in Table 1, while Table 2 lists the values of the proper motions from Tycho-II, TGAS, Gaia DR2 and EDR3 and the resulting $\Delta\mu$.

2.2 Stellar Ages

A full revision of the stellar ages was performed for all the targets following the approaches described in Desidera et al. (2015) and Desidera et al. (2021), considering a variety of indicators and also performing a check for membership to groups using the BANYAN Σ on-line tool³ (Gagné et al. 2018). Most of the targets were found to be field objects, while still compatible with a relatively young age, or

stars with ambiguous membership. In these cases, we considered indirect age indicators such as the equivalent width of 6708Å Lithium doublet, rotation period, X-ray emission, chromospheric activity, taking as reference the empirical sequences of members of groups and clusters (e.g., Desidera et al. 2015) and isochrone fitting. Several of our targets have ages between Hyades and Pleiades. In this range, we took advantage of the recently derived rotation sequence for Group X at an age of 300 Myr (Messina et al. 2022). When applicable, we considered the age indicators for physical companions outside the SPHERE field of view and, for close binaries, we debledended photometric colors for binarity, to improve the reliability of the derived ages. For the few target found to be belonging to young moving groups, we adopted the values of the ages presented in Bonavita et al. (2016) and Desidera et al. (2021), mostly based on Bell et al. (2015). All targets were found to be younger than 1 Gyr, except for GJ 3346 for which the age is likely to be closer to 5 Gyr as discussed in detail in Bonavita et al. (2020). The age determination process for each target is discussed in Appendix A.

2.3 Stellar Masses

The masses for all the stars in the sample were also revised, using the Manifold Age Determination for Young Stars (MADYS, Squicciarini & Bonavita in preparation; see Squicciarini et al. 2021, for a description of the tool) and the updated values of the stellar ages. MADYS retrieved and cross-matched photometry from Gaia EDR3 (Gaia Collaboration et al. 2021) and 2MASS (Skrutskie et al. 2006) for all our targets and then applied a correction for interstellar extinction by integrating along the line of sight the 3D extinction map by (Leike et al. 2020); the derived $A(G)$ were turned into the photometric band of interest using a total-to-selective absorption ratio $R=3.16$ and extinction coefficients A_λ from Wang & Chen (2019). The derived absolute magnitudes were then compared with a grid of isochrones with an age range based on the minimum and maximum age values included in Table 1 to yield a mass estimate. MADYS can use several available grids, but in this instance the PARSEC isochrones (Marigo et al. 2017) were used, due to their large dynamical range spanning the entire stellar regime. A constant solar metallicity, appropriate for most nearby star-forming regions, was assumed (D'Orazi et al. 2011) for all targets except for HIP 21152 and HIP 21317, for which we assumed $[Fe/H]=+0.13$ based on their membership to the Hyades (see Appendix A for details). For each star, a sample of mass estimates was constructed by computing the best-fit mass at different ages within the given age range; its median was taken as the final mass estimate, while the reported errors represent the 16th and the 84 percentile; photometric uncertainties were naturally propagated on the final result via a Monte Carlo approach, i.e. by randomly varying, in a Gaussian fashion, photometric data according to their uncertainties while building the sample of mass estimates.

3 OBSERVATIONS AND DATA REDUCTION

All observations were performed with VLT/SPHERE (Beuzit et al. 2019) with the two Near Infra-Red (NIR) subsystems, IFS (Claudi et al. 2008) and IRDIS (Dohlen et al. 2008) observing in parallel (IRDIFS Mode), with IRDIS in dual-band imaging mode (DBI; Vigan et al. 2010). For all targets we used the IRDIFS-EXT mode, which enables covering the Y -, J -, H -, and K -band in a single observation, which is meant to provide a high-level of spectral content for subsequent analyses.

A summary of the observing parameters and conditions is given in

³ <http://www.exoplanetes.umontreal.ca/banyan/banyansigma.php>

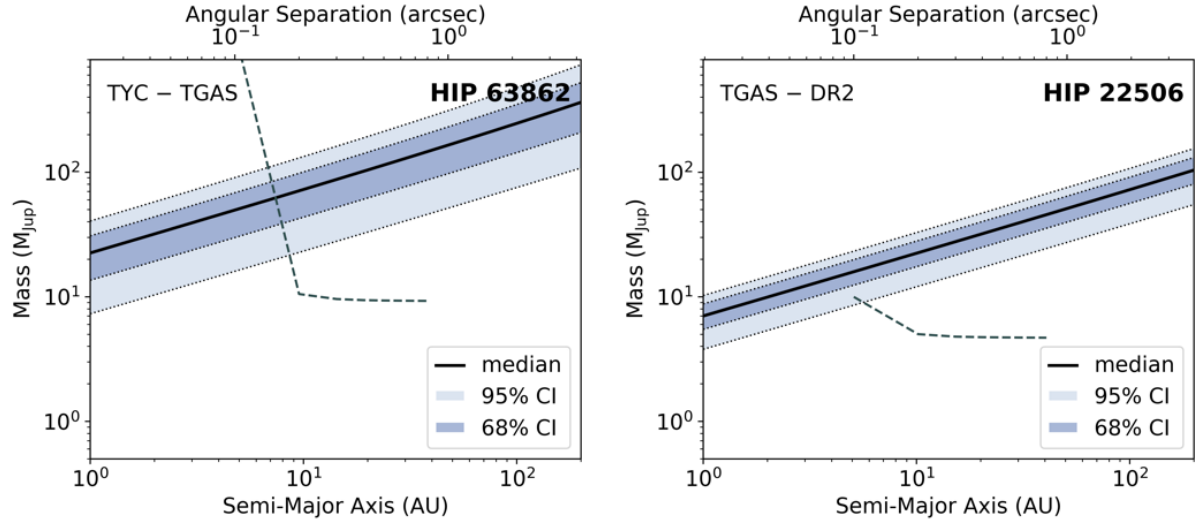


Figure 1. Examples of the solutions computed with COPAINS for the observed astrometric trends of one target selected through the Selection 1 process (using Tycho-2 and TGAS; left) and one target from the Selection 2 process (using TGAS and *Gaia*DR2; right). The solid black lines corresponds to the median curves of solutions, and the dark and light shaded areas represent the 1 and 2- σ confidence intervals, respectively. The dashed grey lines show the expected detection limit used for the survey selection, computed as detailed in the text.

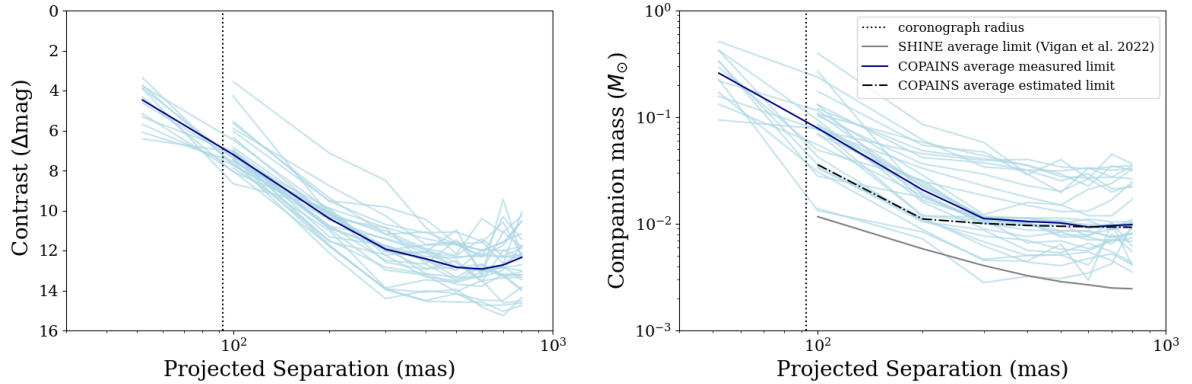


Figure 2. IFS detection limits expressed in contrast (left) and minimum companion mass (right) vs projected separation, for all the targets in our sample. The dashed vertical line marks the coronagraphic radius. Note that objects with multiple epochs will appear more than once. The COND models (Baraffe et al. 2003) were used for the magnitude to mass conversion, using the adopted age from Table 1.

Table 3. The observing sequence adopted was similar to those designed for the SHINE Guaranteed time survey (see e.g. Chauvin et al. 2017) and consisted of:

- One PSF sub-sequence composed of a series of off-axis unsaturated images obtained with an offset of $\sim 0.4''$ relative to the coronagraph center (produced by the Tip-Tilt mirror). A neutral density filter was used to avoid saturation⁴ and the AO visible tip-tilt and high-order loops were closed to obtain a diffraction-limited PSF.
- A *star center* coronagraphic observation with four symmetric satellite spots, created by introducing a periodic modulation on the deformable mirror (see Langlois et al. 2013, for details), in order

to enable an accurate determination of the star position behind the coronagraphic mask for the following deep coronagraphic sequence.

- The deep coronagraphic sub-sequence, for which we used here the smallest apodized Lyot coronagraph (ALC-YH-S) with a focal-plane mask of 185 mas in diameter.
- A new star center sequence, a new PSF registration, as well as a short sky observing sequence for fine correction of the hot pixel variation during the night.

IRDIS and IFS data sets were reduced using the SPHERE Data Reduction and Handling (DRH) automated pipeline (Pavlov et al. 2008) at the SPHERE Data Center (SPHERE-DC, see Delorme et al. 2017) to correct for each data cube for bad pixels, dark current, flat field and sky background. After combining all data cubes with an adequate calculation of the parallactic angle for each individual frame of the deep coronagraphic sequence, all frames are shifted at

⁴ www.eso.org/sci/facilities/paranal/instruments/sphere/inst/filters.html

the position of the stellar centroid calculated from the initial star center position. In order to calibrate the IRDIS and IFS data sets on sky, we used images of the astrometric reference field 47 Tuc observed with SPHERE at a date close to our observations. The plate scale and true north values used are based on the long-term analysis of the GTO astrometric calibration described by [Maire et al. \(2016\)](#).

3.1 Detection Limits

In order to evaluate our sensitivity to stellar companions, we determined detection limits for point sources. We used the standard procedure to derive detection limits outside the coronagraphic field masks that makes use of the SPECAL software as described in [Galicher et al. \(2018\)](#) and used in the F150 survey ([Langlois et al. 2021](#)). The detection limits considered here were obtained using the Template Locally Optimised Combination of Images (TLOCI [Marois et al. 2014](#)) for IRDIS and the ASDI-PCA (Angular Spectral Differential Imaging with PCA [Galicher et al. 2018](#)) for IFS.

Contrast limits for the individual data sets are shown in the left panel of Fig. 2 and reported in Table 4. The corresponding values of the minimum companion mass limits, obtained using the evolutionary models from [Baraffe et al. \(2015\)](#) for the magnitude to mass conversion, are shown in the right panel Fig. 2.

The achieved average limits appear to be significantly worse than the average of the expected limits (dashed-dotted line in Fig. 2) used for the target selection. This is most likely due to the fact that, since our program was executed in service mode and as filler, most of our targets were observed in sub-optimal conditions and with very small field rotation, with a strong negative effect on the quality of the high contrast imaging performances, especially at short separations. This is also confirmed by the fact that the average limit achieved for the first 150 targets of the SHINE survey (gray solid line, from [Vigan et al. \(2021\)](#)), where all target were observed in the best possible conditions, is instead much better than both the measured and estimated COPAINS limits.

4 RESULTS

We detected a total of 14 candidate companions, 4 of which were found to be background sources thanks to additional epochs available in the literature or obtained in our program (HIP 63862, HD 57852, HIP 33690). The 10 co-moving companions are shown in Fig. 3. Eight of the co-moving companions have separations below 0.9 arcseconds, and are therefore in the IFS field of view, while the remaining 2 were only observed with IRDIS. Five are new discoveries, including a white dwarf companion at $\sim 3.6''$ from GJ 3346 (already presented in [Bonavita et al. \(2020\)](#)) and four new sub-stellar companions: HIP 21152 B⁵, HIP 29724 B, HD 60584 B and HIP 63734 B. Their properties are discussed in details in Sec. 4.5, 4.6 and 4.7.

4.1 SPHERE astrometry and photometry

The astrometry and photometry measurements from all our SPHERE observations, are listed in Table 5. For each epoch we report the

projected separation and position angle, and the contrast (expressed as apparent magnitude difference) in the IFS *Y* and *J* filters, as well as the IRDIS *K*₁ and *K*₂ for the IRDIFS-EXT observations⁶. The probability that the source is a background star, evaluated as described in Sec. 4.2, is also listed.

4.2 Common proper motion confirmation

Multiple epochs, used to clarify the bound or background nature of our candidates, were available for 9 of the program stars. Except for HIP 15247 and HD 60584, which were re-observed with SPHERE as part of the program, all additional epochs were retrieved from other surveys, catalogues (including Gaia) or papers dedicated to specific objects. The complete list of astrometric measurements for all our systems is presented in Table 7, together with the references used for each entry. Figure 4 shows the resulting common proper motion analyses for both the co-moving and background interlopers. Note that for HD 60584 we detected two sources, one at 0.5 arcsecs (CC1, discussed in Sec. 4.7) and one at ~ 3 arcsecs (CC2), shown in Fig. 4 and confirmed to be background. The remaining candidates are bright companions at very small separation and are then very likely physically related as the probability of having such bright background stars at these separations is very low. To confirm this, we used the code described in Section 5.2 of [Chauvin et al. \(2015\)](#) and adapted it to our results to estimate the probability of finding a background contaminant at the given separation and contrast as a function of galactic coordinates by comparison with the prediction of the Besançon galactic model ([Robin et al. 2012](#)). As expected all the resulting probabilities (reported in the last column of Table 5) are below 10^{-4} . A further confirmation of common proper motion is also provided by the agreement between the properties of the imaged companions with observed $\Delta\mu$, as discussed in Sec. 4.4.

4.3 Companion spectra

Spectra for the bright companions (providing relatively high SNR data) were obtained using the IFS data. We used the SpEx Prism Library Analysis Toolkit (SPLAT; [Burgasser & Splat Development Team 2017](#)) to estimate the spectral classification of each companion. We used the built-in spectral fitting function in SPLAT to compare, by minimising the χ^2 value, the observed spectra to both the SPLAT near-infrared spectral standards and to the full library of templates available in SPLAT. For bright companions, we simply used the spectrum obtained by rotating and summing the images. For HIP 21152 B, which was not detectable without removing the speckle pattern, we injected negative point spread functions (derived from the flux calibration) on the individual monochromatic images at the average companion position, and changed its intensity minimising the root mean square of the residuals in area of 9×9 pixels centred on this mean position. Figure 5 shows the spectral standard (red) and template (blue) providing the lowest χ^2 values to the observed spectrum of each detected companion. Note that the images of HIP 15247 B was saturated at most wavelengths, so it was not possible to obtain an usable spectrum. Among the five remaining companions, four have an estimated mid- to late-M spectral type, while HIP 21152 B is clearly a substellar object and compatible with a late-L or early-T spectrum.

⁵ HIP 21152 B was independently discovered as part of two other surveys targeting accelerating stars, as detailed in [Kuzuhara et al. \(2022\)](#) and [Franson et al. 2022](#) (in preparation). Both works include an in-depth characterisation of the system, the latter also including a full spectral and orbital analysis combining all available data sets.

⁶ see www.eso.org/sci/facilities/paranal/instruments/sphere/inst/filters.html for a full description of the SPHERE filters.

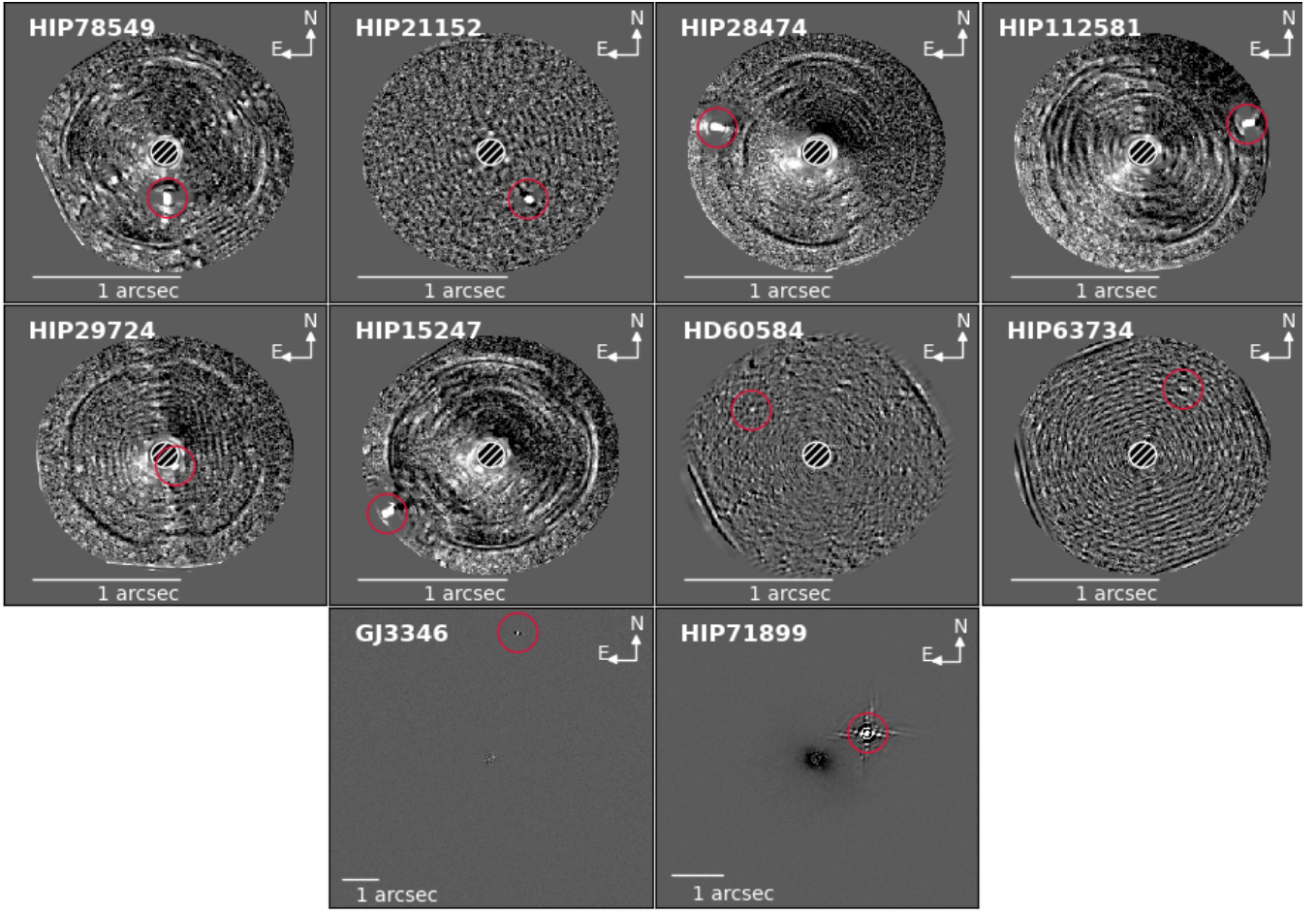


Figure 3. Detected candidate companions in the IFS (top 2 rows) and IRDIS (bottom row) field of view. The red circle marks the position of the candidate.

The strong absorption feature visible in the spectrum of HIP 78549 B is most likely spurious and the result of the extremely low quality of the wavelength calibration available for this object, particularly between 1.32 and 1.45 μm . We therefore masked this region of the spectrum while performing the fit. The resulting mid M spectral type is in agreement with the properties estimated from the photometry.

4.4 FORECAST (Finely Optimised REtrieval of Companions of Accelerating STars)

Since the $\Delta\mu$ can be considered as an approximation of the instantaneous acceleration due to an unseen companion, it can be represented as a vector in the plane of the sky directed toward the position of the companion - at the epoch of the latest astrometry observation. The position angle of an imaged companion compatible with the $\Delta\mu$ should then be along the same direction of the acceleration, plus or minus the change in angle due to the orbital motion of the companion between the latest astrometry epoch and the imaging one. Based on these considerations, it is possible to highlight a region on the plane of the sky where the companion compatible with the $\Delta\mu$ should lie, based on the $\Delta\mu$ orientation, and also associate a value of the companion mass corresponding to each point in the resulting 2D map, based on the $\Delta\mu$ absolute value. An example of the $\Delta\mu$ maps obtained with this method using the $\Delta\mu$ at the epoch of *Gaia* EDR3 (2016.0) is shown in Fig. 6, while a complete description of the method, and of the FORECAST (Finely Optimised REtrieval of Companions of

Accelerating STars) code used to produce the maps will be the subject of a dedicated companion publication (Bonavita et al. 2022, in preparation). In each image, the position of the detected companion is marked as a star. As all companions lie within the allowed region (as shown in the left panel of Fig. 7, which compares the PAs of the companions and those of the $\Delta\mu$ vectors), we could also obtain a first estimate the expected companion mass at that position and compare it with the values of the value of the mass derived from the photometry. The dynamical masses ($M_{\Delta\mu}$) were estimated using the method described in Kervella et al. (2019), which allows to also take into account the effect of the unknown orbital eccentricity and inclination, as well as that of the observing window smearing, which are instead not taken into account by the COPAINS tool. The comparison with the photometric masses (M_{Phot}) is shown in the right panel of Fig. 7, with the error bars on the values of $M_{\Delta\mu}$ taking into account the errors on the $\Delta\mu$ and companion position, and those on M_{Phot} mainly arising from the uncertainties on the stellar ages. The good agreement between the values shows the potential of our method in providing a high number of potential new benchmark objects.

4.5 HIP 21152 B: a new bound substellar companion in the Hyades

The companion to HIP 21152 is clearly the most interesting of our high SNR detections. The IRDIS photometry and the IFS spectra, shown in Fig. 5, point towards an early T spectral type. The

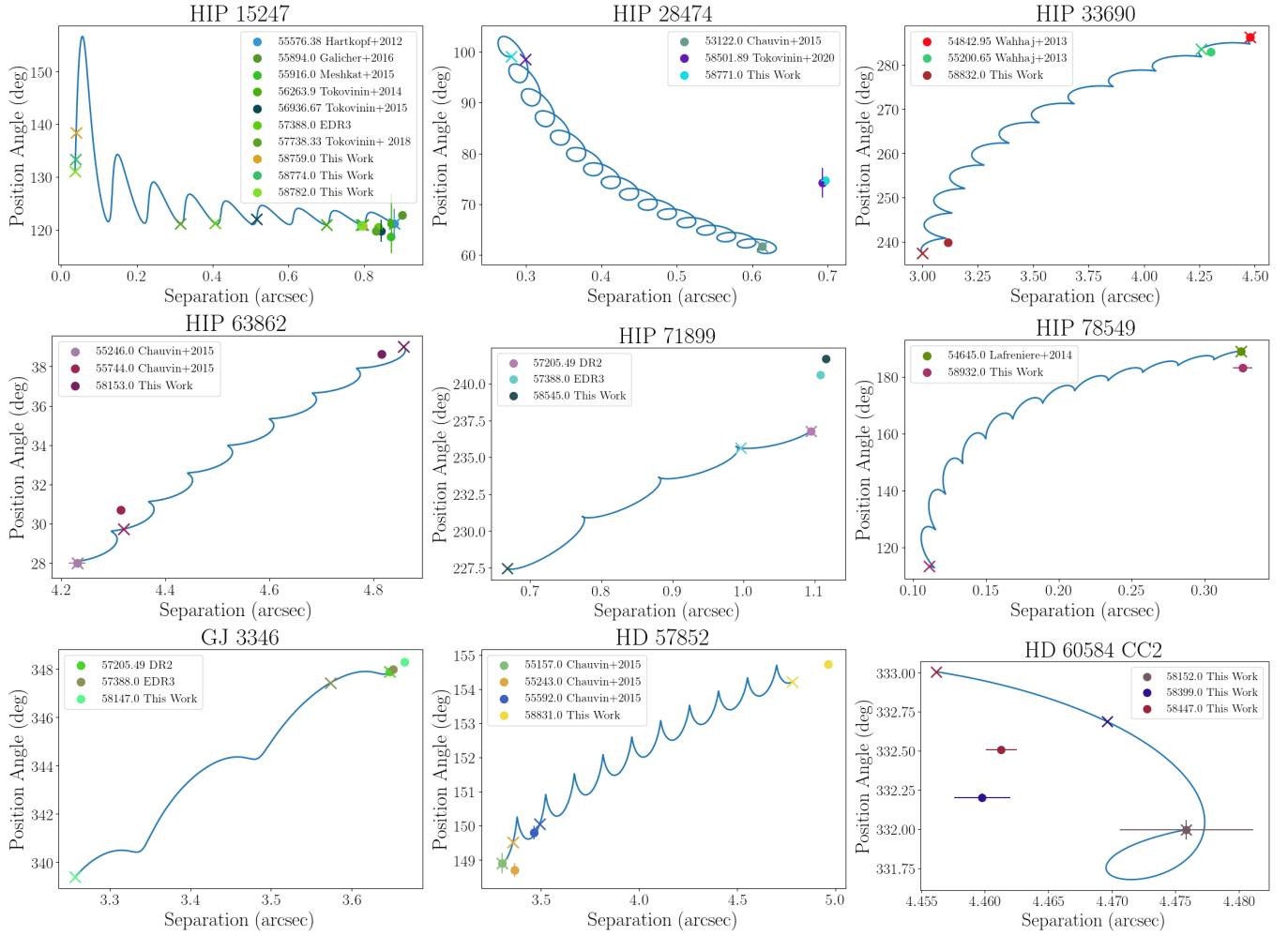


Figure 4. Common proper motion analysis of all our candidate companions with multiple epochs (reported in Table 7). The blue line shows the motion of a background object relative to the target, based on the EDR3 parallax and proper motion of the primary over the same time frame. In all panels, the filled circles show the measured separation and position angle of the companions at each epoch, colour coded as explained in the legends. The crosses indicates the expected position of a background object at the same epoch, following the same colour code. The companions for HIP 28474, HIP 78549, HIP 15274, HIP 71899 and GJ 3346 (updated from the dedicated work published in Bonavita et al. (2020), which only included *Gaia*DR2 epoch), are clearly found to be co-moving with our targets.

mass of the object, as judged from its spectral type and age, and adopting the models from Baraffe et al. (2015)⁷, is estimated to be $0.032 \pm 0.005 M_{\odot}$. This is also in good agreement with the mass derived from the FORECAST analysis, which is $0.021 \pm 0.007 M_{\odot}$. The Lithium-depletion boundary, an observational limit that separates low-mass stars from brown dwarfs based on their ability to burn Li in their cores, has been estimated to occur around spectral type L3.5 - L4 in Hyades (Martín et al. 2018). Currently, about a dozen objects with spectral type L3.5 or later claimed as members of the cluster. Lodieu et al. (2014) published spectra of 12 L-dwarf candidates from Hogan et al. (2008), and confirmed one of them as a potential brown dwarf member of Hyades, with spectral type

L3.5. The same objects has later been listed as a L4 member of Hyades, with Li absorption detected in the spectra by Martín et al. (2018). Four more L-type members (two L5 and two L6) have been confirmed in Schneider et al. (2017); Pérez-Garrido et al. (2017, 2018). Bouvier et al. (2008) were the first to report the existence of T-type candidate members in Hyades. The membership of one of them (CFHT-Hy-21) has been confirmed by Lodieu et al. (2014), whereas the other one (CFHT-Hy-20) is still considered a candidate (Lodieu et al. 2014; Zhang et al. 2021), given the lack of radial velocity measurement. Four T-type probable members have been reported in Zhang et al. (2021), spanning the spectral type range T2 to T6.5. The multiplicity of Hyades stars has been assessed through imaging (Reid & Gizis 1997; Patience et al. 1998; Siegler et al. 2003; Duchêne et al. 2013), high-resolution spectroscopy (Reid & Mahoney 2000), a combination of the two (Guenther et al. 2005), and *Gaia* astrometry (Deacon & Kraus 2020). While several binary systems consisting of two substellar objects, or objects close to the (sub)stellar border, were reported in Siegler et al. (2003); Reid & Mahoney (2000); Duchêne et al. (2013), no substellar companions to FGK stars have so far been reported in Hyades, making HIP 21152 B

⁷ New atmospheric models have been recently developed by Phillips et al. (2020). However, such models (known as ATMO2020) are mostly valid for relatively old ultra-cool objects (late-T and Y companions). Therefore, given the age and brightness of HIP 21152 B as well as the estimated spectral type, we decided that the models from Baraffe et al. (2015) would be more suited for the mass estimate in this case. The same applies to the other BD companions described in Sec. 4.6 and 4.7

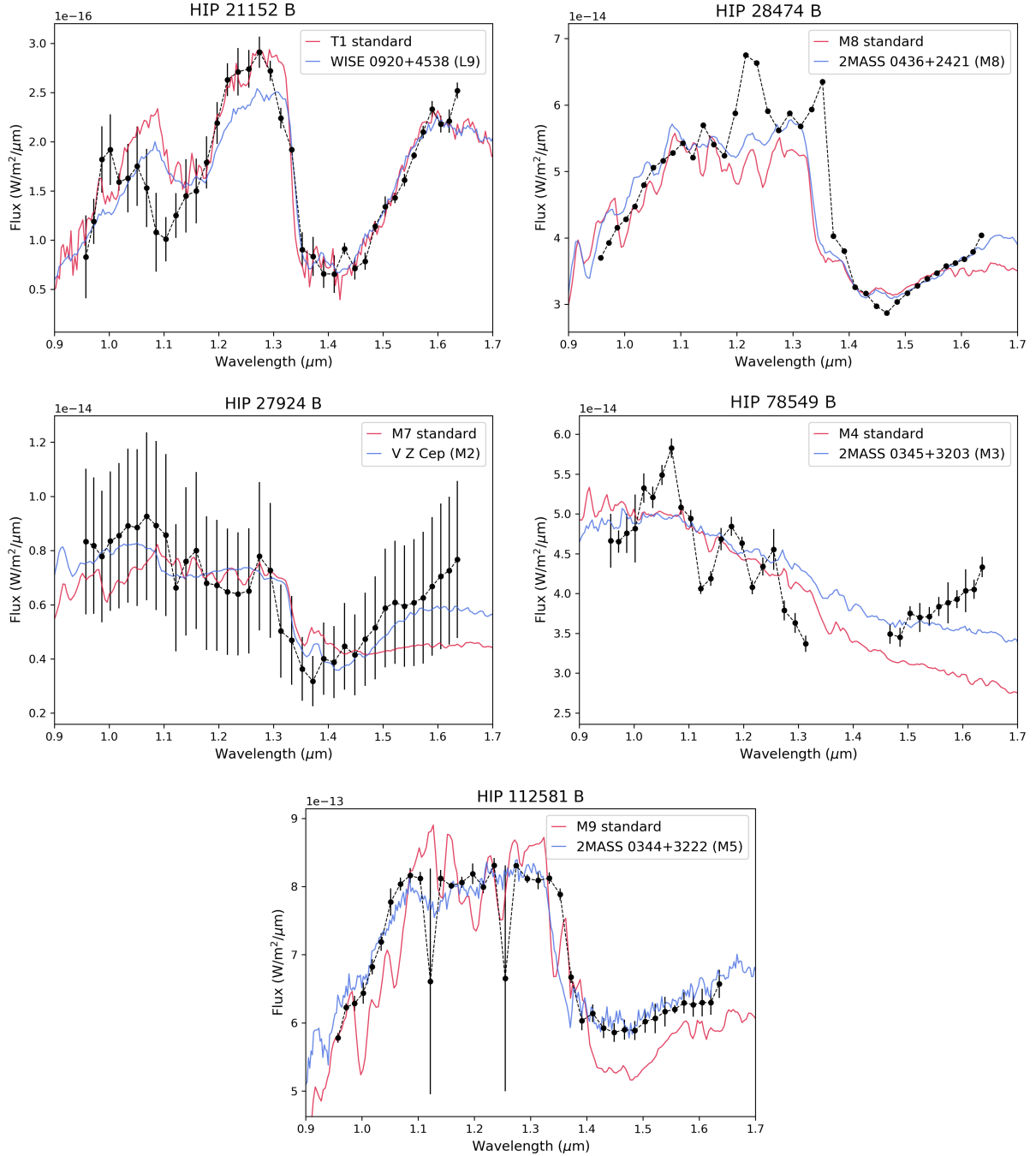


Figure 5. Comparison between the spectra of five of the companions detected at high SNR (black bullets with error bars) with the best fit from SPLAT (Burgasser & Splat Development Team 2017), showing in red the best fit among the spectral standards provided in SPLAT, and in blue the overall best fit among all available templates.

the first of its kind. HIP 22152 B thus occupies a unique place in the luminosity-age parameter space compared to the known population of directly-imaged systems, making it a highly valuable benchmark for empirical constraints to theoretical models.

BD companions such HIP 22152 B have been shown in the past to be themselves close pairs of substellar objects (see e.g. Martín et al. 2000; Potter et al. 2002) and optimised PSF subtraction methods have been recently developed to highlight the presence of close companions to BDs detected with SPHERE (see e.g. Lazzoni

et al. 2020). Such methods rely on the detection and analysis of features such as elongation in the companion’s PSF incompatible with the expected effects of ADI. Although a detailed analysis would benefit from a new set of higher quality data, we can say that no such features were detected in our images for HIP 21152 B. Moreover, to be on stable orbits, possible additional companions would need to have separations within HIP 21152 B’s Hill Radius, which we estimated to be roughly at 3.57 au, for the optimistic case of a circular orbit. At the distance of HIP 21152 B (~ 43 pc), this

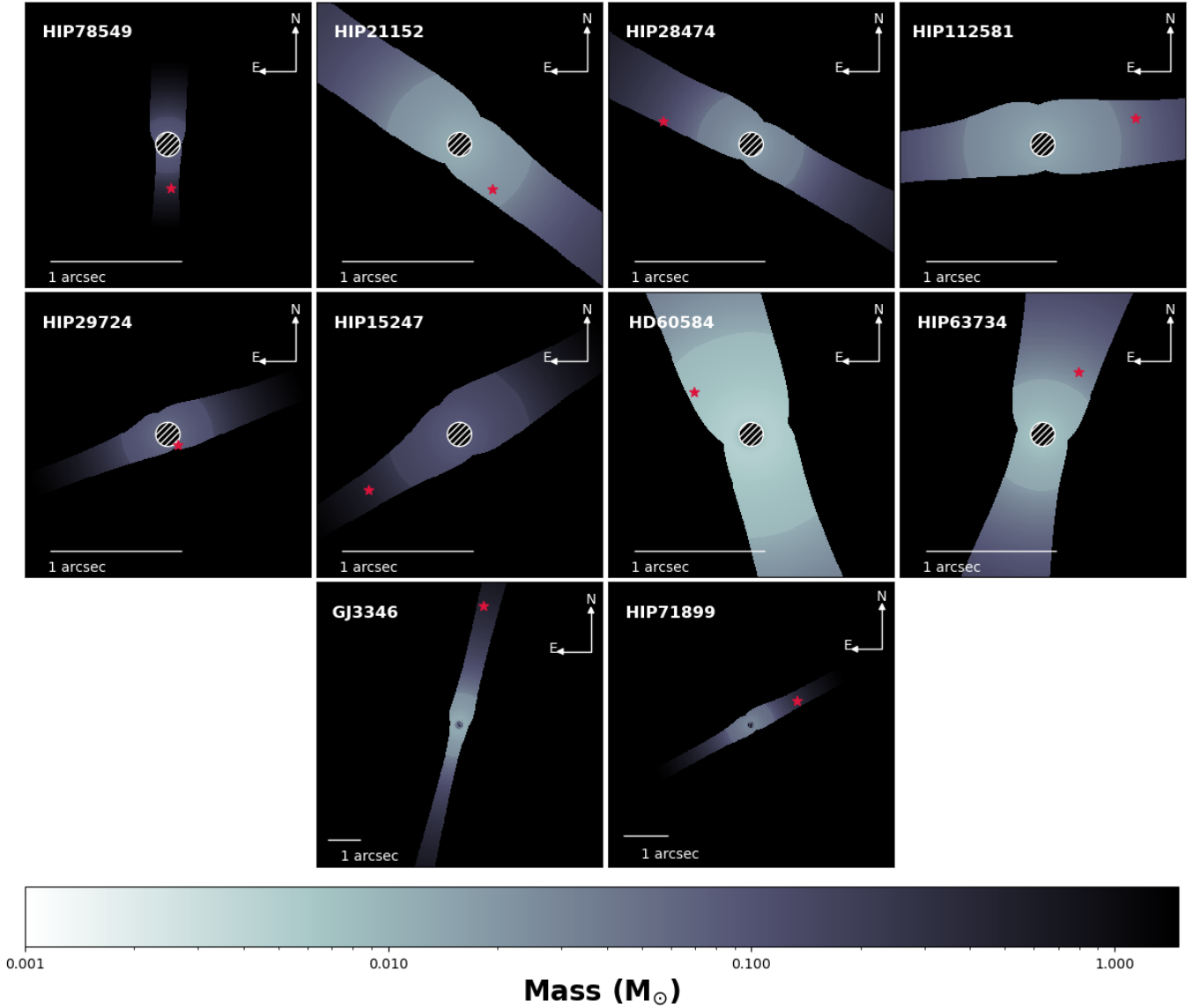


Figure 6. 2D maps representing the sky area compatible with the TGAS-EDR3 $\Delta\mu$ reported in Table 2. The position of the companions is marked with a red star. Colours are according to the dynamical mass responsible for the $\Delta\mu$ at a give distance; the same logarithmic scale was used for all stars, according to the colour scale shown on the bottom of the figure. The empty area at center is the area covered by the coronagraphic mask.

corresponds to a projected separation of roughly 82 mas. While this target has good potential for the detection of additional (possibly less massive) companions, an analysis like the one described by Lazzoni et al. (2020) will require higher quality data than those presented in this work.

4.6 HIP 29724 B: a new high mass brown dwarf

We also detected a very close (99.9 ± 1.5 mas) companion to HIP 29724. The photometry suggests a mass of $0.063 \pm 0.008 M_{\odot}$, thus placing HIP 29724 B also in the sub-stellar regime. The FORECAST analysis confirms that the companion is compatible with the observed TGAS-EDR3 $\Delta\mu$, both in terms of position and corresponding mass ($0.067 \pm 0.021 M_{\odot}$). With a projected separation of just 6.3 au, RV monitoring could significantly contribute to the refinement of the BD orbit and dynamical mass. However, there are no high-

precision RV measurements available up to now. Sparse RV data over several decades (Nordström et al. 2004; Torres et al. 2006; Gaia Collaboration et al. 2018) are constant within 1.2 km/s. The spectrum of the companion, shown in Fig. 5, is compatible with a late M spectral type, although a later spectral type is not completely excluded, given the uncertainties caused by the companion's proximity to the edge of the coronagraph.

As it was the case for HIP 21152 B, the PSF of HIP 29724 B does not show any elongation beyond what expected as result of the ADI. We estimated for this companion an Hill Radius of 1.71 au (27.2 mas, assuming a circular orbit) thus limiting the detectability of possible additional companions to roughly equal-mass ones, considering the spatial resolution of our images.

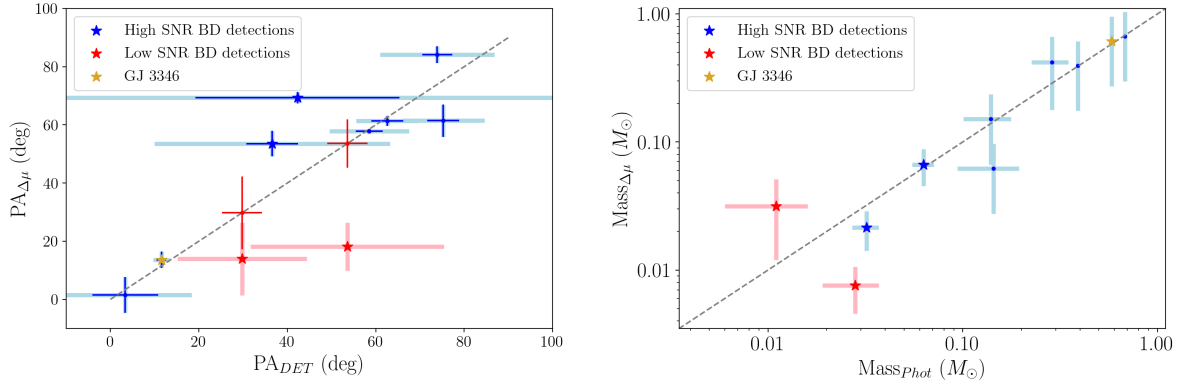


Figure 7. Left Panel: PA of the detected companions VS the direction of the $\Delta\mu$. The shaded error bars show the extend of the expected change in angle due to the orbital motion between the SPHERE observation and the *Gaia* EDR3 epoch. **Right Panel:** Comparison between the values of the mass of the detected companions derived using FORECAST, and those obtained from photometry and evolutionary models (as described in Sec. 2.3). Both values of the masses are reported in Table 8 for all companions. In both panels blue symbols are high SNR detections; red symbols are low SNR candidates that needs further confirmation.

4.7 HD 60584 B and HIP 63734 B: two more potential low mass brown dwarf candidate companions

The $\Delta\mu$ maps obtained with FORECAST are not only useful to confirm the nature of the candidates found in objects with highly significant $\Delta\mu$, but could in principle also be used as *finding charts* to highlight and retrieve possible additional companions appearing in the imaging data at a SNR lower than the threshold required for a confirmed detection, which would otherwise be overlooked. We had in fact noticed that all our high SNR detections were around stars for which the ratio between the $\Delta\mu$ absolute value and its error (hereafter $SNR_{\Delta\mu}$) is higher than 10. So we decided to produce the FORECAST maps also for the targets with low or intermediate SNR_{Max} (HD 60584, HIP 63734, and HIP 22506) as a test for their possible use as *finding charts*.

While the data for HIP 63734 were taken in fairly good atmospheric conditions, the target was observed quite far from meridian passage so that field rotation is limited (only 7.13 degrees). The analysis of the IFS data with ASDI-PCA revealed a candidate companion with $SNR \sim 8.5$, at separation 555 ± 2 mas and $PA = 329.6 \pm 0.2$ degree, with a contrast of $dJ = 12.08$ and $dH = 11.26$. The comparison with Baraffe et al. (2003) models yields an evolutionary mass of $0.011 \pm 0.005 M_\odot$. While the PA of the object is fully compatible with that of the $\Delta\mu$, the corresponding companion mass is a bit higher ($0.032 \pm 0.020 M_\odot$) is a bit higher than the evolutionary one. However, this detection is uncertain because the small rotation angle makes the noise distribution quite different from a Gaussian.

The case of HD 60584 is slightly more complicated. Although there were four available epochs, the resulting IFS data were all of relatively poor quality. The second and third epochs were taken at about one month interval; since we did not expect a large orbital motion between them, we combined them as a single observation. This allowed us to identify a point source compatible with the FORECAST predictions at a separation 543 ± 5 mas and $PA = 52.5 \pm 0.5$ degrees, with a SNR of 4.9. At that position, the mass of a companion compatible with the $\Delta\mu$ would have to be below $0.01 M_\odot$ which, at the relatively high age of the targets would mean that the companion would have to be fairly faint. While the IFS photometry points towards a higher mass ($0.028 \pm 0.009 M_\odot$), given the high uncertainties due to the image and calibration quality and the very field small rotation angle we still

deemed it acceptable. As for the other BDs, no evident elongation pointing towards possible additional companions was observed for the PSF of HIP 63734 B and HD 60584 B. However, given the low SNR of the detections, we estimate that the only potentially detectable companions within the Hill Radius of these BDs (103 and 80 mas, respectively) would have been equal-mass ones.

Although further investigation is required to confirm the nature of both HD 60584 B and HIP 63734 B, mostly due to the poor quality of the imaging data, these additional detections clearly show the power of the approach, which pushes the $\Delta\mu$ method towards companions with smaller masses, whose detection is more uncertain and likely to be below the usual 10σ threshold used for automatic retrieval of point sources in imaging data. Although repeated observations will be needed to confirm low SNR imaging detections, with the use of FORECAST a single observation is potentially enough to confirm that a companion observed in high contrast imaging is the one responsible for the $\Delta\mu$, and therefore co-moving. Other low SNR point sources were retrieved around HIP 22506, but were discarded mostly based on the strong disagreement between their brightness and the value of the mass compatible with the position within the FORECAST map. This also shows the power of FORECAST in terms of vetting of possible background or spurious sources.

5 DISCUSSION

The COPAINS selection method has proven very successful in ensuring a high detection rate in both the stellar and sub-stellar regime. We detected a total of 14 candidate companions. Two were known binaries (HIP 15247 B and HIP 78549 B) and four were identified as background sources thanks to additional available epochs found in the literature, which also allowed us to confirm the common proper motion nature of four additional new stellar companions, including the white dwarf companion to GJ 3346, described in Bonavita et al. (2020). The masses of the remaining four candidates, derived using the available photometry and the evolutionary models from Baraffe et al. (2015), place them in the sub-stellar regime. Such high sub-stellar companion detection rate confirms the efficiency of the COPAINS selection method, as well as the new FORECAST code

used to confirm their nature, based on the agreement between their properties with the predictions based on the measured $\Delta\mu$.

5.1 Comparison with blind surveys

To quantify the improvement in terms of detection rate compared to blind surveys, we compared our results with those from the first 150 targets from the SHINE survey (Vigan et al. 2021). Only 93 of the SHINE-150 targets are included in TGAS and DR2, and only 13 have $\Delta\mu$ more significant than 3σ , and would have therefore been selected for COPAINS. Three of these SHINE $\Delta\mu$ stars have sub-stellar companions, including HIP 65426, one of the two new SHINE detections. The resulting sub-stellar companions frequency is then $\sim 25\%$ which is significantly higher than what obtained with the blind approach ($\sim 9\%$ without any correction due to prior knowledge about the companions, see Vigan et al. (2021) for details), once again showing the efficiency of the COPAINS selection method, especially when combined with the FORECAST maps.

5.2 Limitations

We have demonstrated with our campaign the power of using informed target selection processes such as the COPAINS tool (Fontanive et al. 2019) to identify new directly-imaged companions. The high detection rate obtained here strongly validates the use of such approaches in survey designs, despite the numerous assumptions and limitations of the work conducted in this pilot survey. Indeed, our original sample selection considered catalogue proper motions taken at face value. Instead, a more accurate approach would require placing all measurements in the same reference frame and at the same epoch, such as the Hipparcos-*Gaia* Catalog of Accelerations (HGCA) defined by Brandt (2018, 2021). These catalogues provides Hipparcos and *Gaia* DR2/EDR3 proper motions, as well as a *Gaia*-Hipparcos scaled positional differences (close to the TGAS proper motions), placing all proper motions at the epochs of *Gaia*DR2 and EDR3, respectively, with recalibrated uncertainties. Nonetheless, given the number of approximations made in COPAINS, these differences were found to be negligible, especially given the use made of the resulting computed trends (i.e., visual selection based on comparisons to expected detection limits). As COPAINS considers long-term proper motions as representative of the system's center-of-mass motion, and short-term measurements as the instantaneous reflex motion of the host, the considered $\Delta\mu$ are only good approximations for systems with orbital periods that roughly match the long- and short-term timescales of the considered astrometric catalogues (see Fontanive et al. 2019). These limitations are further added to the adopted eccentricity distribution, primarily impacting the width of the computed solutions, and the fact that the approach assumes face-on orbits, which implies that estimated trends actually provide lower mass limits for a given separation. While information from the now available HGCA catalogues (Brandt 2018, 2021) or proper motion anomalies measured by Kervella et al. (2019, 2022) would therefore provide more robust and reliable astrometric trends to use for selection purposes (and should consistently be used for orbital and dynamical mass constraints), our results were not impacted by the use of uncorrected catalogue values, and we have nonetheless shown that the idea behind our method offers a highly promising pathway for future observing programs.

6 CONCLUSIONS

We presented the results of the COPAINS survey, a search for companions to 25 stars selected using the COPAINS tool by Fontanive et al. (2019), and the discovery of four new brown dwarf companions: HIP 21152 B, HIP 29724 B, HD 60584 B and HIP 63734 B.

The value of blind surveys of course lies in their ability to constrain the underlying planet and sub-stellar companion population, but comes with a high cost in terms of telescope time. On the other hand, surveys like COPAINS offer an undeniably efficient selection method, providing a much higher success rate with a considerably smaller time commitment. Moreover, the possibility to derive model independent mass estimates for the companions to accelerating stars also means that each new detection arising from surveys like COPAINS can be added to the currently scarce number of much needed benchmark objects, providing new crucial constraints the evolutionary models. Given the good agreement between the values of the masses of these companions obtained from the photometry with the model-independent ones based on the $\Delta\mu$, this work represents a considerable addition to the current benchmarks sample.

The combination with the FORECAST maps ensures a high detection rate even when the quality of the imaging data is not ideal, while at the same time further enhancing the sensitivity to lower mass companions. Fig. 8 shows the mass ratio (left panel) and companion mass (right panel) vs separation of the COPAINS sub-stellar candidates compared to those of the known DI companions (data from exoplanet.eu updated on April 4th, 2022). An estimate of the $\Delta\mu$ was possible for about 40% of the known companions and about half of these (shown as coloured dots in Fig. 8) would have been selected using COPAINS. This plot once again shows how a selection like the one provided by COPAINS can already lead to the detection of companions well in the planetary mass regime.

Catalogues like those by Brandt et al. (2019) and Kervella et al. (2022) provide a more robust estimate of the accelerations, and therefore their use with COPAINS is likely to lead to an even more effective selection. Moreover, these acceleration catalogues can also be used to retrieve a time series of absolute astrometry which, combined with the imaging data, allows for a more detailed characterisation of the orbit, and thus of the dynamical mass (see e.g. Drimmel et al. 2021). The availability of *Gaia*-only accelerations in the upcoming full third *Gaia*Release (DR3) will allow for another great step further. It will in fact not only free the method from the boundaries so far imposed by the use of external catalogue as source of long term proper motion, but more importantly will allow for a significant improvement in terms of uncertainties, thus allowing future survey to truly focus on targets with accelerations caused by planetary mass companion.

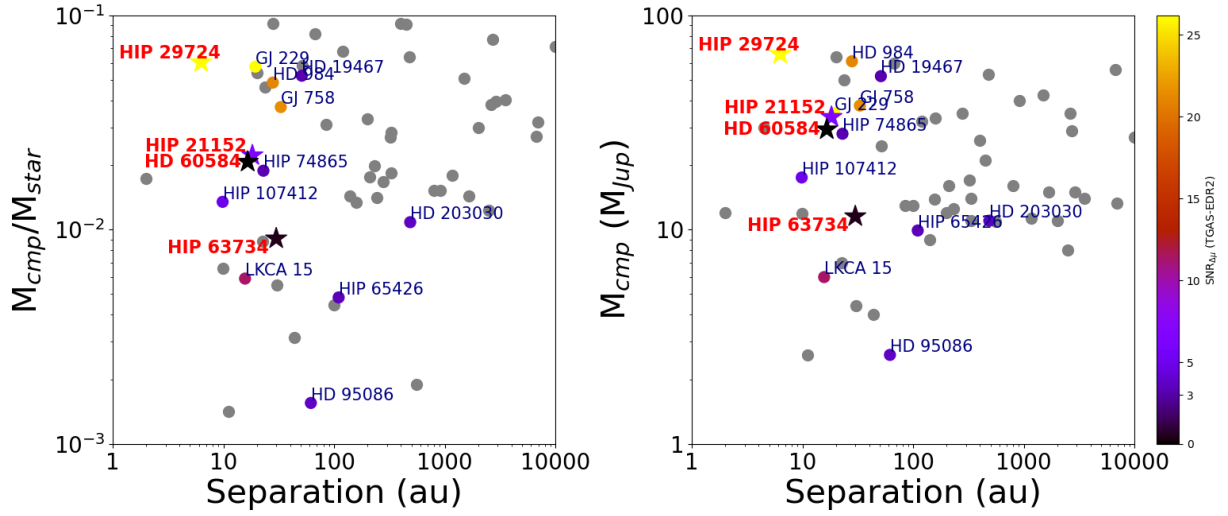


Figure 8. Mass ratio (M_{cmp}/M_{star} , left panel) and companion mass (M_{Jup} , right panel) vs separation (in au) of the four COPAINS sub-stellar candidates (star symbols) compared to those of previously known DI companions (filled circles). The colour bar shows the significance of the TGAS-DR2 $\Delta\mu$ ($SNR_{\Delta\mu}$) used for the COPAINS selection. Objects with $SNR_{\Delta\mu} < 3$ (or not in TGAS, and therefore without a measurement of the $\Delta\mu$) are shown in gray.

Table 1. Sample characteristics. All the values of the parallax are from *Gaia*EDR3. The values of the age (Age_{\min}^{\max}) and stellar mass ($\text{Mass}_{\min}^{\max}$) are derived as described in Sec. 2.2 and 2.3 (see also Appendix A for details on the age derivation for the single objects). The last column includes the observing period for which the target was originally proposed for and therefore the selection method applied, as detailed in Section 2.1

ID	RA (hh:mm:ss)	Dec (°:′:″)	Parallax (mas)	SpType	<i>J</i> mag	<i>H</i> mag	<i>K</i> mag	Age _{min} ^{max} Myr	Mass _{min} ^{max} M _☉	Sel
HIP 15247	1:10:09.411	-3:31:48.575	20.37 ± 0.03	F6V	6.457	6.209	6.099	45 ₃₀ ¹⁵⁰	1.23 _{-0.003} ^{0.006}	P104
HIP 17439	3:44:09.0243	-38:16:56.771	61.84 ± 0.02	K2V	5.462	5.088	4.934	700 ₅₀₀ ⁹⁰⁰	0.87 _{-0.001} ^{0.001}	P104
HIP 21152	4:32:04.7457	5:24:36.069	23.11 ± 0.03	F5V	5.593	5.385	5.333	625 ₆₀₀ ⁷⁰⁰	1.44 _{-0.002} ^{0.002}	P104
HIP 21317	4:34:35.2511	15:30:16.873	21.67 ± 0.02	F8	6.745	6.552	6.445	625 ₆₀₀ ⁷⁰⁰	1.12 _{-0.001} ^{0.001}	P100
HIP 22506	4:50:35.4147	-41:02:51.426	19.83 ± 0.05	G9V	7.438	7.099	6.876	50 ₄₀ ¹²⁵	0.96 _{-0.009} ^{0.002}	P104
GJ 3346	5:19:59.4774	-15:50:24.411	42.09 ± 0.02	K3.5Vk:	6.856	6.284	6.205	5400 ₄₃₀₀ ⁶⁵⁰⁰	0.74 _{-0.003} ^{0.003}	P100
HIP 27441	5:48:36.7913	-39:55:55.814	23.59 ± 0.01	K0V	7.407	7.061	6.912	250 ₁₅₀ ³⁵⁰	0.90 _{-0.001} ^{0.001}	P100
HIP 28474	6:00:41.2853	-44:53:50.304	18.48 ± 0.01	G8V	7.73	7.433	7.321	42 ₃₅ ¹²⁵	0.96 _{-0.020} ^{0.001}	P104
HIP 29724	6:15:38.8408	-57:42:05.96	15.86 ± 0.01	G2V	7.715	7.447	7.346	150 ₁₀₀ ²⁵⁰	1.04 _{-0.001} ^{0.001}	P104
HIP 33690	6:59:59.8409	-61:20:12.444	54.53 ± 0.01	G9V	5.459	5.097	4.987	650 ₅₀₀ ⁸⁰⁰	0.94 _{-0.002} ^{0.001}	P104
HD 57852	7:20:21.4547	-52:18:42.709	28.63 ± 0.23	F5V	5.28	5.13	4.946	200 ₁₅₀ ³⁰⁰	1.41 _{-0.006} ^{0.006}	P104
HD 60584	7:34:18.6723	-23:28:25.17	32.75 ± 0.04	F5V+F6V	5.03	4.9	4.773	1000 ₃₀₀ ¹⁷⁰⁰	1.35 _{-0.016} ^{0.012}	P100
HIP 52462	10:43:28.4085	-29:03:51.014	46.49 ± 0.02	K1V	6.176	5.77	5.66	170 ₁₂₀ ²⁵⁰	0.86 _{-0.001} ^{0.001}	P104
HIP 56153	11:30:35.5865	-57:08:02.252	44.53 ± 0.02	K3.5V(k)	6.495	6.019	5.868	700 ₅₀₀ ¹⁰⁰⁰	0.79 _{-0.001} ^{0.001}	P102
HIP 59726	12:14:57.6323	-41:08:21.243	31.14 ± 0.02	G5V	6.31	6.008	5.925	700 ₅₀₀ ¹⁰⁰⁰	1.02 _{-0.003} ^{0.002}	P104
HIP 61804	12:40:00.1103	-17:41:03.596	16.20 ± 0.31	G3V	7.295	7.043	6.869	120 ₈₀ ²⁰⁰	1.12 _{-0.010} ^{0.009}	P104
HIP 63734	13:03:39.0733	-16:20:11.414	18.49 ± 0.03	F7/8V	6.752	6.522	6.436	150 ₁₀₀ ³⁰⁰	1.21 _{-0.006} ^{0.006}	P104
HIP 63862	13:05:16.9255	-50:51:23.776	21.06 ± 0.02	G6V	7.158	6.834	6.744	200 ₁₂₀ ³⁰⁰	1.03 _{-0.002} ^{0.001}	P100
HIP 71899	14:42:23.1023	21:17:35.386	21.94 ± 0.02	F8	6.447	6.223	6.172	300 ₁₀₀ ³⁰⁰⁰	1.18 _{-0.012} ^{0.011}	P102
HIP 78549	16:02:13.5632	-22:41:15.023	7.01 ± 0.03	B9.5V	7.037	7.038	6.97	11 ₄ ¹²	2.61 _{-0.014} ^{0.010}	P104
HIP 108912	22:03:42.303	-60:26:14.87	23.38 ± 0.02	G2V	6.773	6.529	6.444	300 ₂₀₀ ⁴⁰⁰	1.07 _{-0.002} ^{0.002}	P104
HIP 112491	22:47:09.1673	-32:40:30.874	36.43 ± 0.02	G8V	6.295	5.958	5.852	700 ₅₀₀ ⁹⁰⁰	0.95 _{-0.002} ^{0.001}	P104
HIP 112581	22:48:06.8092	-37:45:23.989	26.14 ± 0.02	G0VCH-0.3	6.415	6.172	6.1	600 ₄₅₀ ⁸⁰⁰	1.09 _{-0.003} ^{0.002}	P104
CD-69 2101	23:31:00.5329	-69:05:09.756	33.03 ± 0.01	K3V	7.345	6.824	6.712	350 ₂₀₀ ⁵⁰⁰	0.77 _{-0.001} ^{0.001}	P100
HIP 116768	23:39:54.9912	9:40:38.345	14.05 ± 0.29	A2m	5.563	5.488	5.471	780 ₅₂₀ ¹⁰⁴⁰	1.88 _{-0.062} ^{0.045}	P104

Table 2. Proper motion values from TGAS, DR2 and EDR3 and the resulting $\Delta\mu$ values obtained considering TGAS or Tycho-II as source for long term proper motions and DR2 or EDR3 as sources short-term proper motions.

ID	pmRA				pmDE				$\Delta\mu$		
	TYCHO-2	TGAS	DR2	EDR3	TYCHO-2	TGAS	DR2	EDR3	TYC-TGAS	TGAS-DR2	TGAS-DR3
HIP 15247	77.70 ± 1.40	79.25 ± 0.04	82.10 ± 0.09	82.10 ± 0.03	-45.80 ± 1.30	-47.25 ± 0.03	-49.08 ± 0.08	-49.05 ± 0.03	2.13 ± 0.05	3.39 ± 0.09	3.36 ± 0.05
HIP 17439	209.90 ± 1.20	209.07 ± 0.04	208.91 ± 0.03	209.06 ± 0.02	291.00 ± 1.20	289.26 ± 0.05	289.30 ± 0.05	289.32 ± 0.02	1.93 ± 0.05	0.16 ± 0.05	0.06 ± 0.05
HIP 21152	113.20 ± 1.30	112.59 ± 0.04	112.50 ± 0.13	112.17 ± 0.03	5.40 ± 1.30	8.06 ± 0.02	7.58 ± 0.06	7.76 ± 0.02	2.73 ± 0.04	0.49 ± 0.06	0.51 ± 0.04
HIP 21317	98.10 ± 1.00	101.12 ± 0.10	100.87 ± 0.11	100.96 ± 0.03	-26.70 ± 1.10	-26.74 ± 0.06	-26.86 ± 0.07	-26.81 ± 0.02	3.02 ± 0.10	0.28 ± 0.14	0.18 ± 0.10
HIP 22506	37.10 ± 1.10	36.77 ± 0.04	36.45 ± 0.13	36.46 ± 0.06	69.90 ± 1.10	69.08 ± 0.05	68.07 ± 0.14	68.59 ± 0.07	0.88 ± 0.08	1.06 ± 0.15	0.58 ± 0.08
GJ 3346	174.30 ± 1.30	174.02 ± 0.06	173.57 ± 0.05	173.70 ± 0.01	201.20 ± 1.40	206.39 ± 0.06	207.56 ± 0.06	207.71 ± 0.01	5.20 ± 0.07	1.25 ± 0.08	1.35 ± 0.07
HIP 27441	26.50 ± 1.10	28.43 ± 0.05	28.46 ± 0.05	28.43 ± 0.01	71.10 ± 1.30	66.48 ± 0.05	66.21 ± 0.05	66.38 ± 0.01	5.01 ± 0.06	0.27 ± 0.07	0.11 ± 0.06
HIP 28474	16.80 ± 1.00	17.52 ± 0.07	18.15 ± 0.05	18.22 ± 0.01	21.10 ± 1.10	23.09 ± 0.08	23.26 ± 0.05	23.47 ± 0.01	2.12 ± 0.07	0.65 ± 0.08	0.79 ± 0.07
HIP 29724	30.20 ± 1.30	29.41 ± 0.07	27.67 ± 0.04	27.51 ± 0.02	48.30 ± 1.30	47.79 ± 0.07	48.46 ± 0.04	48.50 ± 0.02	0.94 ± 0.08	1.86 ± 0.08	2.02 ± 0.08
HIP 33690	-160.80 ± 1.30	-161.89 ± 0.04	-162.07 ± 0.05	-161.87 ± 0.02	266.30 ± 1.60	264.87 ± 0.04	264.64 ± 0.04	264.84 ± 0.02	1.80 ± 0.04	0.29 ± 0.06	0.04 ± 0.04
HD 57852	-62.50 ± 1.20	-36.88 ± 0.05	-37.71 ± 0.59	-37.05 ± 0.32	107.00 ± 1.50	146.69 ± 0.05	148.39 ± 0.56	146.29 ± 0.29	47.24 ± 0.30	1.89 ± 0.56	0.43 ± 0.30
HD 60584	-83.50 ± 1.10	-88.05 ± 0.04	-88.13 ± 0.07	-88.13 ± 0.02	-0.80 ± 1.00	-0.59 ± 0.04	-0.74 ± 0.09	-0.86 ± 0.04	4.55 ± 0.05	0.17 ± 0.09	0.28 ± 0.05
HIP 52462	-212.50 ± 1.50	-215.57 ± 0.03	-215.54 ± 0.06	-215.48 ± 0.01	-50.00 ± 1.20	-49.88 ± 0.04	-50.12 ± 0.06	-49.89 ± 0.02	3.08 ± 0.04	0.24 ± 0.07	0.09 ± 0.04
HIP 56153	-553.30 ± 2.00	-555.35 ± 0.07	-555.29 ± 0.17	-555.33 ± 0.02	36.40 ± 1.50	36.13 ± 0.06	35.91 ± 0.22	36.13 ± 0.02	2.07 ± 0.07	0.23 ± 0.22	0.02 ± 0.07
HIP 59726	-312.80 ± 0.90	-313.95 ± 0.04	-313.90 ± 0.05	-313.97 ± 0.02	-78.50 ± 0.90	-77.04 ± 0.03	-77.17 ± 0.03	-77.00 ± 0.01	1.86 ± 0.03	0.14 ± 0.05	0.04 ± 0.03
HIP 61804	-48.00 ± 1.30	-45.70 ± 0.07	-47.83 ± 0.38	-46.64 ± 0.34	-10.40 ± 1.40	-11.60 ± 0.05	-12.23 ± 0.32	-11.15 ± 0.22	2.59 ± 0.33	2.22 ± 0.38	1.04 ± 0.33
HIP 63734	-108.70 ± 1.20	-108.30 ± 0.05	-108.48 ± 0.10	-108.37 ± 0.03	-28.90 ± 1.10	-29.55 ± 0.03	-29.31 ± 0.07	-29.30 ± 0.02	0.76 ± 0.04	0.30 ± 0.09	0.26 ± 0.04
HIP 63862	-135.50 ± 1.10	-134.34 ± 0.04	-134.15 ± 0.11	-134.34 ± 0.02	-1.10 ± 1.10	-4.45 ± 0.05	-4.65 ± 0.08	-4.45 ± 0.02	3.54 ± 0.05	0.28 ± 0.11	0.00 ± 0.05
HIP 71899	-108.00 ± 1.00	-107.27 ± 0.03	-108.39 ± 0.06	-108.42 ± 0.01	-31.50 ± 1.00	-34.51 ± 0.04	-35.21 ± 0.07	-35.14 ± 0.02	3.10 ± 0.03	1.32 ± 0.07	1.31 ± 0.03
HIP 78549	-12.00 ± 1.40	-12.54 ± 0.04	-12.51 ± 0.11	-12.53 ± 0.03	-24.70 ± 1.40	-23.13 ± 0.03	-23.53 ± 0.06	-23.65 ± 0.02	1.66 ± 0.03	0.40 ± 0.06	0.52 ± 0.03
HIP 108912	105.30 ± 1.40	106.47 ± 0.05	106.27 ± 0.04	106.40 ± 0.01	2.10 ± 1.40	2.08 ± 0.05	2.20 ± 0.05	2.00 ± 0.02	1.17 ± 0.05	0.23 ± 0.07	0.11 ± 0.05
HIP 112491	248.00 ± 1.30	247.31 ± 0.07	247.14 ± 0.08	247.28 ± 0.02	-90.60 ± 1.20	-91.24 ± 0.05	-90.86 ± 0.06	-91.25 ± 0.02	0.94 ± 0.07	0.42 ± 0.09	0.02 ± 0.07
HIP 112581	158.30 ± 1.60	156.54 ± 0.05	155.64 ± 0.07	155.72 ± 0.02	1.90 ± 1.20	1.49 ± 0.04	1.71 ± 0.08	1.57 ± 0.02	1.81 ± 0.05	0.93 ± 0.08	0.82 ± 0.05
CD-69 2101	186.90 ± 1.50	181.14 ± 0.63	185.55 ± 0.04	185.66 ± 0.01	-124.50 ± 1.40	-125.88 ± 0.75	-126.36 ± 0.05	-126.53 ± 0.02	5.92 ± 0.64	4.43 ± 0.64	4.56 ± 0.64
HIP 116768	88.60 ± 1.50	88.17 ± 0.05	86.91 ± 0.36	87.50 ± 0.28	-11.30 ± 1.50	-10.20 ± 0.04	-10.18 ± 0.28	-10.50 ± 0.19	1.18 ± 0.28	1.26 ± 0.36	0.74 ± 0.28

Table 3. Summary of VLT/SPHERE observations.

ID	OBS DATE	MJD	MODE	DITxNDIT	ND Filt	FoV rot	seeing	τ_0
HIP 15247	2019-10-03	58759.27718	IRDIFS-EXT	64x2	ND 3.5	19.54	0.89	0.0021
	2019-10-18	58774.26027	IRDIFS-EXT	64x2	ND 3.5	2.13	1.03	0.0024
	2019-10-26	58782.22189	IRDIFS-EXT	64x2	ND 3.5	25.60	1.0	0.0026
HIP 17439	2019-10-02	58758.30404	IRDIFS-EXT	32x6	ND 3.5	49.90	1.06	0.0022
HIP 21152	2019-10-26	58782.29206	IRDIFS-EXT	64x3	ND 3.5	36.63	1.19	0.0032
	2019-10-26	58782.29206	IRDIFS-EXT	64x3	ND 3.5	36.63	1.19	0.0032
HIP 21317	2019-03-03	58545.34589	IRDIFS-EXT	64x1	ND 2.0	5.93	0.93	0.0043
HIP 22506	2019-10-03	58759.31361	IRDIFS-EXT	64x3	ND 3.5	31.72	0.98	0.0018
GJ 3346	2018-01-29	58147.10689	IRDIFS-EXT	64x1	ND 2.0	5.16	1.18	0.0039
HIP 27441	2018-10-03	58394.32920	IRDIFS-EXT	64x1	ND 2.0	6.63	1.22	0.003
HIP 28474	2019-10-16	58772.26844	IRDIFS-EXT	64x3	ND 3.5	31.85	1.2	0.002
	2019-10-28	58784.31147	IRDIFS-EXT	64x3	ND 3.5	37.70	1.01	0.0038
HIP 29724	2019-10-12	58768.32106	IRDIFS-EXT	64x2	ND 3.5	12.38	1.04	0.0028
HIP 33690	2019-12-05	58822.24603	IRDIFS-EXT	64x3	ND 3.5	19.75	0.93	0.0033
HD 57852	2019-12-14	58831.24541	IRDIFS-EXT	64x3	ND 3.5	27.11	0.93	0.0089
HD 60584	2018-02-03	58152.24399	IRDIFS-EXT	64x1	ND 3.5	0.84	1.01	0.0064
	2018-10-08	58399.33920	IRDIFS-EXT	64x1	ND 3.5	1.82	1.05	0.0024
	2018-11-25	58447.22078	IRDIFS-EXT	64x1	ND 3.5	0.82	0.91	0.0084
	2019-12-16	58833.30235	IRDIFS-EXT	32x5	ND 3.5	1.62	1.68	0.0027
HIP 52462	2020-01-04	58852.23233	IRDIFS-EXT	32x6	ND 3.5	6.28	1.22	0.0097
HIP 56153	2019-02-03	58545.27470	IRDIFS-EXT	16x4	ND 2.0	0.41	1.05	0.005
HIP 59726	2020-01-08	58856.26851	IRDIFS-EXT	64x3	ND 3.5	2.98	1.29	0.0015
	2020-01-19	58867.24264	IRDIFS-EXT	64x3	ND 3.5	11.37	1.02	0.0124
HIP 61804	2020-02-22	58901.28462	IRDIFS-EXT	64x2	ND 3.5	57.53	1.13	0.0051
HIP 63734	2020-02-07	58886.27393	IRDIFS-EXT	64x3	ND 3.5	6.36	1.15	0.0041
HIP 63862	2018-02-04	58153.34083	IRDIFS-EXT	64x1	ND 2.0	9.25	1.0	0.0079
HIP 71899	2019-03-03	58545.34590	IRDIFS-EXT	64x1	ND 2.0	5.93	0.93	0.0043
HIP 78549	2020-03-24	58932.30214	IRDIFS-EXT	32x6	ND 3.5	8.62	1.24	0.0042
HIP 108912	2019-10-04	58760.06723	IRDIFS-EXT	64x3	ND 3.5	20.45	1.25	0.0021
HIP 112491	2019-10-02	58758.18845	IRDIFS-EXT	64x2	ND 3.5	6.99	1.28	0.0009
HIP 112581	2019-10-04	58760.13838	IRDIFS-EXT	64x3	ND 1.0	27.74	0.81	0.003
CD-69 2101	2017-10-01	58027.12834	IRDIFS-EXT	64x1	ND 2.0	6.12	0.99	0.0034
HIP 116768	2019-10-05	58761.11277	IRDIFS-EXT	64x2	ND 3.5	16.74	0.8	0.0023

Table 4. IFS contrast limits (expressed as Δmag) for all the available data sets.

ID	JD	52mas	100mas	200mas	300mas	400mas	500mas	600mas	700mas	800mas
HIP 15247	03/10/2019		7.49	10.08	11.96	12.9	12.86	12.68	13.23	13.94
HIP 15247	18/10/2019		6.04	9.52	9.82	10.44	11.66	11.61	10.59	12.25
HIP 15247	26/10/2019	3.89	7.36	9.9	12.25	13.32	13.52	13.1	12.79	13.46
HIP 17439	02/10/2019	5.17	8.03	11.76	13.92	14.09	13.95	14.83	15.26	14.35
HIP 21152	26/10/2019	6.09	7.53	12.13	14.41	14.01	14.15	14.49	14.5	13.83
HIP 21317	02/02/2018		6.85	10.24	11.03	11.9	12.25	11.41	12.29	11.88
HIP 71899	03/03/2019		7.26	10.75	12.5	12.68	13.49	12.81	13.26	13.24
HIP 22506	03/10/2019		7.88	11.01	13.88	13.47	13.59	13.25	12.66	10.1
GJ 3346	29/01/2018		7.17	11.55	12.22	12.11	12.86	13.03	12.86	12.72
HIP 27441	03/10/2018		5.54	9.55	10.7	11.11	11.07	11.54	12.65	12.14
HIP 28474	16/10/2019	3.36	7.76	10.16	11.98	11.73	11.69	12.33	10.31	11.44
HIP 28474	28/10/2019	3.77	6.47	10.0	12.05	12.09	10.96	13.27	9.44	12.33
HIP 29724	12/10/2019	3.91	8.66	9.88	10.86	11.41	11.71	11.97	12.0	11.8
HIP 33690	05/12/2019	6.42	7.07	11.72	13.96	14.54	14.58	14.58	15.04	14.75
HD 57852	14/12/2019	4.62	7.37	11.8	13.92	14.5	14.16	14.74	14.73	14.63
HD 60584	03/02/2018		6.34	10.35	10.87	12.68	11.47	13.02	11.06	11.82
HD 60584	08/10/2018		7.0	11.32	11.74	12.3	12.38	12.15	12.32	12.2
HD 60584	25/11/2018		7.24	10.77	11.41	11.94	12.62	13.56	11.99	12.31
HD 60584	16/12/2019		7.56	10.12	11.18	11.97	12.83	12.95	12.87	13.0
HIP 52462	04/01/2020		7.47	10.86	11.81	13.16	13.33	12.69	13.26	14.0
HIP 56153	02/03/2019		6.98	10.47	11.44	12.08	12.31	12.29	11.75	10.54
HIP 59726	08/01/2020		3.56	7.13	8.5	10.84	12.17	10.41	11.1	10.27
HIP 61804	22/02/2020	3.74	7.68	11.5	12.84	13.16	13.69	13.79	13.17	13.22
HIP 63734	07/02/2020		7.12	10.88	11.91	12.44	13.36	13.33	12.99	11.74
HIP 63862	04/02/2018		4.28	10.21	12.05	12.39	12.85	12.91	13.29	13.06
HIP 78549	24/03/2020		5.9	8.76	10.27	11.7	11.59	12.03	11.57	11.15
HIP 108912	04/10/2019	4.33	8.07	10.08	12.59	12.95	12.5	13.51	13.37	13.34
HIP 112491	02/10/2019									
HIP 112581	04/10/2019	5.69	7.73	10.45	11.77	12.52	13.0	11.98	11.6	10.53
CD-69 2101	01/10/2017		5.65	9.37	11.18	11.08	11.69	12.26	12.32	12.36
HIP 116768	05/10/2019	5.33	7.04	10.92	12.98	13.23	14.06	13.49	14.62	14.52

Table 5. SPHERE astrometry and photometry for all the candidate companions detected in our sample. Each epoch is reported separately. The last two columns show the status of the candidate and the probability of finding a background contaminant at the given separation and contrast as a function of galactic coordinates, derived as described in Sec. 4.2.

ID	Obs. Date (MJD)	ρ (mas)	PA ($^\circ$)	IFS Photometry		IRDIS Photometry		Status	Bkg Prob
				ΔY	ΔJ	ΔK_1	ΔK_2		
HIP 15247	58759.2772	810.10 ± 1.50	121.30 ± 0.11			2.02 ± 0.03	2.15 ± 0.12	C1	$1.79 \cdot 10^{-7}$
	58774.2603	810.10 ± 1.50	121.30 ± 0.11		3.56 ± 0.50	2.15 ± 0.03	2.16 ± 0.14		
	58782.2219	808.80 ± 1.50	121.50 ± 0.10		3.65 ± 0.50	2.11 ± 0.03	2.34 ± 0.22		
GJ 3346	58147.1069	3665.02 ± 2.27	348.31 ± 1.42			7.84 ± 1.63	7.79 ± 0.06	C1	$2.05 \cdot 10^{-4}$
HIP 21152	58782.2921	422.40 ± 1.50	217.06 ± 0.20	11.65 ± 0.50	11.92 ± 0.50	10.82 ± 0.04	10.86 ± 0.05	C0	$8.17 \cdot 10^{-7}$
HIP 28474	58772.2684	696.80 ± 1.50	75.42 ± 0.12	3.46 ± 0.50	3.75 ± 0.50	3.71 ± 0.03	3.63 ± 0.02	C1	$4.05 \cdot 10^{-6}$
	58784.3115	694.40 ± 1.50	75.44 ± 0.12	3.77 ± 0.50	3.61 ± 0.50				
HIP 29724	58768.3211	99.90 ± 1.50	214.00 ± 0.86	5.81 ± 0.50	6.36 ± 0.50	5.63 ± 0.20	6.00 ± 0.70	C0	$6.57 \cdot 10^{-7}$
HIP 33690	58822.246	3117.57 ± 1.10	239.87 ± 0.87			5.41 ± 0.01	7.70 ± 0.17	B2	
HD 57852	58831.2454	4792.45 ± 6.50	20.18 ± 0.30			20.18 ± 3.67	15.88 ± 1.81	B2	
HD 60584 CC1	58447.2208	543.00 ± 5.00	52.50 ± 0.50		12.70 ± 0.50			L	$8.34 \cdot 10^{-4}$
HD 60584 CC2	58152.244	4475.87 ± 5.24	332.00 ± 0.06			10.05 ± 0.01	10.00 ± 0.01	B1	
	58399.3392	4459.78 ± 2.21	332.20 ± 0.03			10.41 ± 0.09	10.35 ± 0.06		
	58447.2208	4461.29 ± 1.23	332.51 ± 0.02			9.94 ± 0.04	10.65 ± 0.02		
HIP 63734	58886.2739	555.00 ± 2.00	329.60 ± 0.20	11.26 ± 0.50	12.08 ± 0.50			L	$5.30 \cdot 10^{-5}$
HIP 63862	58153.3408	4815.57 ± 5.67	38.62 ± 0.06			12.72 ± 0.11	12.33 ± 0.45	B2	
HIP 71899	58545.3459	1115.91 ± 4.50	241.69 ± 0.05			3.72 ± 0.01	3.98 ± 0.11	C1	$3.39 \cdot 10^{-6}$
HIP 78549	58932.3021	333.20 ± 1.50	183.40 ± 0.26	4.24 ± 0.50	4.68 ± 0.50	9.58 ± 0.65	12.37 ± 1.35	C1	$2.52 \cdot 10^{-6}$
HIP 112581	58760.1384	736.80 ± 1.50	286.30 ± 0.12	4.71 ± 0.50	5.00 ± 0.50	5.48 ± 0.01	5.32 ± 0.01	C0	$2.17 \cdot 10^{-6}$

Status: C0 = bound companion based on statistical arguments; C1 = bound companion based on additional epochs from other works; B0 = background based on statistical arguments; B1 = background based on follow-up from this work; B2 = background based on additional epochs from other works; U = L = Low SNR detection (see Sec. 4.4)

Table 6. Gaia astrometry and photometry of companions retrieved in EGDR3, including additional companions outside SPHERE FoV. Separations and position angles were derived using the positions from Gaia EDR3, when available. Further details about the known systems can be found in Appendix A. The ID of the target is reported in the first column to be consistent with the rest of the tables in the paper. The Gaia ID, and the values of the parallax and proper motion reported are those retrieved in EDR3 for the companions. Although the companions of HIP 15247 and HD 129501 were detected by Gaia, no astrometric solution was available in EDR3 (hence the blank fields).

ID _A	Gaia EDR3 ID _B	parallax (mas)	Proper Motion		Δ mag Gaia G band	separation (arcsec)	PA ($^\circ$)
			RA (mas/yr)	DEC (mas/yr)			
HIP 15247	Gaia EDR3 3261733202649353216					0.84	120.56
HIP 24874	Gaia EDR3 2983256662868370048	42.240 ± 0.035	182.685 ± 0.031	216.203 ± 0.032	14.331	3.65	347.98
HIP 27441	Gaia EDR3 4805207967655791488	23.675 ± 0.013	31.712 ± 0.014	65.198 ± 0.014	12.303	33.98	113.54
HD 60584	Gaia EDR3 5618420137803146240	32.792 ± 0.035	-87.258 ± 0.016	-11.556 ± 0.036	5.758	9.95	117.61
HD 57852	Gaia EDR3 5492026740698525696	29.476 ± 0.449	-31.762 ± 0.546	138.163 ± 0.567	6.465	9.05	26.72
HIP 71899	Gaia EDR3 1241384331822285184				12.936	1.11	240.59

Table 7. Complete list of all the astrometric data for the detected candidate companions for which more than one epoch was available, with the appropriate references listed in the last column.

ID	Obs.Date (MJD-245000)	rho (mas)	e_{rho} (mas)	PA (°)	e_{PA} (°)	Ref.
HIP 15247	55576.4	0.879	0.003	121.15	2.80	Hartkopf+2012
	55894.0	0.900	0.010	122.80	0.10	Galicher+2016
	55916.0	0.870	0.010	118.67	0.49	Meshkat+2015
	56263.9	0.872	0.006	121.20	5.70	Tokovinin+2014
	56936.7	0.844	0.003	119.80	2.10	Tokovinin+2015
	57388.0	0.837	0.001	120.55	0.02	EDR3
	57738.3	0.830	0.001	119.80	0.90	Tokovinin+ 2018
	58759.0	0.796	0.004	120.71	0.05	This Work
	58774.0	0.792	0.004	120.89	0.05	This Work
	58782.0	0.793	0.004	120.77	0.05	This Work
GJ 3346	57205.5	3.647	0.001	347.89	0.02	DR2
	57388.0	3.651	0.001	347.98	0.02	EDR3
	58147.0	3.665	0.002	348.30	0.07	This Work
HIP 28474	53122.0	0.613	0.003	61.70	0.20	Chauvin+2015
	58501.9	0.693	0.003	74.20	2.90	Tokovinin+2020
	58771.0	0.697	0.005	74.73	0.24	This Work
HIP 33690	54842.9	4.479	0.009	286.20	0.20	Wahhaj+2013
	55200.6	4.302	0.009	282.90	0.20	Wahhaj+2013
	58832.0	3.117	0.007	239.85	0.01	This Work
HD 57852	55157.0	3.301	0.020	148.90	0.30	Chauvin+2015
	55243.0	3.365	0.013	148.70	0.20	Chauvin+2015
	55592.0	3.465	0.009	149.80	0.20	Chauvin+2015
	58831.0	4.962	0.006	154.73	0.12	This Work
HD 60584	58152.0	4.476	0.005	331.10	0.06	This Work
	58399.0	4.460	0.002	332.20	0.03	This Work
	58447.0	4.461	0.001	332.51	0.02	This Work
HIP 63862	55246.0	4.231	0.016	28.00	0.20	Chauvin+2015
	55744.0	4.315	0.005	30.70	0.10	Chauvin+2015
	58153.0	4.815	0.006	38.62	0.05	This Work
HIP 71899	57205.5	1.094	0.001	236.78	0.02	DR2
	57388.0	1.108	0.001	240.59	0.02	EDR3
	58545.0	1.116	0.004	241.69	0.05	This Work
HIP 78549	54645.0	0.325	0.001	189.06	0.19	Lafreniere+2014
	58932.0	0.326	0.007	183.17	1.08	This Work

Table 8. Summary of the characteristics of the comoving companions. If more than one SHINE epoch was available, only the separation (ρ) and position angle (PA) from the first epoch are reported, information on the single measurements for these objects can be found in Tab. 5.

Except for GJ 3346, for which we used the values from Bonavita et al. (2020), the masses of the primaries (M_A) were derived as described in Sec. 2.3. The same is true for $M_B(\text{phot})$, which is the value of the secondary mass obtained from the photometry, using the COND models (Baraffe et al. 2003). $M_B(\Delta\mu)$ is instead the value of the secondary mass inferred using FORECAST (see Sec. 4.4 for details).

ID	Separation		PA (deg)	M_A (M_\odot)	$M_B(\text{phot})$ (M_\odot)	$M_B(\Delta\mu)$ (M_\odot)	Notes
	(mas)	(au)					
HIP 15247	810.10 ± 1.50	39.78 ± 0.09	121.30 ± 0.11	1.228 ± 0.004	0.680 ± 0.015	0.668 ± 0.369	WD
HIP 21152	422.40 ± 1.50	18.28 ± 0.07	217.06 ± 0.20	1.442 ± 0.002	0.032 ± 0.005	0.021 ± 0.007	
GJ 3346	3665.02 ± 2.27	87.07 ± 0.06	348.31 ± 1.42	0.683 ± 0.018	0.580 ± 0.010	0.611 ± 0.339	
HIP 28474	696.80 ± 1.50	37.71 ± 0.08	75.42 ± 0.12	0.958 ± 0.011	0.139 ± 0.038	0.152 ± 0.085	
HIP 29724	99.90 ± 1.50	6.30 ± 0.09	214.00 ± 0.86	1.044 ± 0.001	0.063 ± 0.008	0.067 ± 0.021	Low SNR
HD 60584	543.00 ± 5.00	16.58 ± 0.15	232.50 ± 0.50	1.352 ± 0.014	0.028 ± 0.009	0.008 ± 0.003	
HIP 63734	555.00 ± 2.00	30.02 ± 0.12	329.60 ± 0.20	1.211 ± 0.006	0.011 ± 0.003	0.032 ± 0.020	Low SNR
HIP 71899	1115.91 ± 4.50	50.85 ± 0.21	241.69 ± 0.05	1.178 ± 0.012	0.390 ± 0.005	0.393 ± 0.218	
HIP 78549	333.20 ± 1.50	47.52 ± 0.30	183.40 ± 0.26	2.614 ± 0.012	0.284 ± 0.064	0.420 ± 0.241	
HIP 112581	736.80 ± 1.50	28.19 ± 0.06	286.30 ± 0.12	1.091 ± 0.003	0.144 ± 0.050	0.062 ± 0.035	

DATA AVAILABILITY

The data used for this work are available through the ESO Science Archive Facility (<http://archive.eso.org/cms.html>).

REFERENCES

- Andersen J., Nordstrom B., 1983, *A&AS*, **52**, 471
- Baraffe I., Chabrier G., Barman T. S., Allard F., Hauschildt P. H., 2003, *A&A*, **402**, 701
- Baraffe I., Homeier D., Allard F., Chabrier G., 2015, *A&A*, **577**, A42
- Bell C. P. M., Mamajek E. E., Naylor T., 2015, *MNRAS*, **454**, 593
- Beuzit J. L., et al., 2019, *A&A*, **631**, A155
- Biller B. A., et al., 2007, *ApJS*, **173**, 143
- Biller B. A., et al., 2013, *ApJ*, **777**, 160
- Bonavita M., de Mooij E. J. W., Jayawardhana R., 2013, *PASP*, **125**, 849
- Bonavita M., Desidera S., Thalmann C., Janson M., Vigan A., Chauvin G., Lannier J., 2016, *A&A*, **593**, A38
- Bonavita M., et al., 2020, *MNRAS*, **494**, 3481
- Bouvier J., et al., 2008, *A&A*, **481**, 661
- Bowler B. P., 2016, *PASP*, **128**, 102001
- Bowler B. P., Blunt S. C., Nielsen E. L., 2020, *AJ*, **159**, 63
- Bowler B. P., et al., 2021, *AJ*, **161**, 106
- Brandt T. D., 2018, *ApJS*, **239**, 31
- Brandt T. D., 2021, *ApJS*, **254**, 42
- Brandt T. D., Dupuy T. J., Bowler B. P., 2019, *AJ*, **158**, 140
- Burgasser A. J., Splat Development Team 2017, in *Astronomical Society of India Conference Series*. pp 7–12 ([arXiv:1707.00062](https://arxiv.org/abs/1707.00062))
- Calissendorff P., Janson M., 2018, *A&A*, **615**, A149
- Casagrande L., Schönrich R., Asplund M., Cassisi S., Ramírez I., Meléndez J., Bensby T., Feltzing S., 2011, *A&A*, **530**, A138
- Chauvin G., et al., 2010, *A&A*, **509**, A52
- Chauvin G., et al., 2015, *A&A*, **573**, A127
- Chauvin G., et al., 2017, *A&A*, **605**, L9
- Chen C. H., Mittal T., Kuchner M., Forrest W. J., Lisse C. M., Manoj P., Sargent B. A., Watson D. M., 2014, *ApJS*, **211**, 25
- Chilcote J., et al., 2021, *AJ*, **162**, 251
- Chupina N. V., Reva V. G., Vereshchagin S. V., 2006, *A&A*, **451**, 909
- Claudi R. U., et al., 2008, in *Proc. SPIE*. p. 70143E, [doi:10.1117/12.788366](https://doi.org/10.1117/12.788366)
- Currie T., et al., 2020, *ApJ*, **904**, L25
- D’Orazi V., Biazzo K., Randich S., 2011, *A&A*, **526**, A103
- Deacon N. R., Kraus A. L., 2020, *MNRAS*, **496**, 5176
- Delorme P., et al., 2017, *A&A*, **608**, A79
- Desidera S., Gratton R. G., Lucatello S., Claudi R. U., Dall T. H., 2006, *A&A*, **454**, 553
- Desidera S., et al., 2015, *A&A*, **573**, A126
- Desidera S., et al., 2021, *A&A*, **651**, A70
- Dohlen K., et al., 2008, in *Proc. SPIE*. p. 70143L, [doi:10.1117/12.789786](https://doi.org/10.1117/12.789786)
- Dommanget J., Nys O., 2002, *VizieR Online Data Catalog*, **p. I/274**
- Drimmel R., Sozzetti A., Schröder K.-P., Bastian U., Pinamonti M., Jack D., Hernández Huerta M. A., 2021, *MNRAS*, **502**, 328
- Duchêne G., Bouvier J., Moraux E., Bouy H., Konopacky Q., Ghez A. M., 2013, *A&A*, **555**, A137
- Dupuy T. J., Brandt T. D., Kratter K. M., Bowler B. P., 2019, *ApJ*, **871**, L4
- ESA 1997, *VizieR Online Data Catalog*, **1239**, 0
- Ertel S., et al., 2014, *A&A*, **561**, A114
- Fontanive C., Mužić K., Bonavita M., Biller B., 2019, *MNRAS*, **490**, 1120
- Gagné J., Faherty J. K., 2018, *ApJ*, **862**, 138
- Gagné J., Roy-Loubier O., Faherty J. K., Doyon R., Malo L., 2018, *ApJ*, **860**, 43
- Gaia Collaboration et al., 2016, *A&A*, **595**, A1
- Gaia Collaboration et al., 2018, *A&A*, **616**, A1
- Gaia Collaboration Brown A. G. A., Vallenari A., Prusti T., de Bruijne J. H. J., et al. 2021, *A&A*, **649**, A1
- Galicher R., et al., 2016a, *A&A*, **594**, A63
- Galicher R., et al., 2016b, *A&A*, **594**, A63
- Galicher R., et al., 2018, *A&A*, **615**, A92
- Golimowski D. A., et al., 2011, *AJ*, **142**, 30
- Grandjean A., et al., 2019, *A&A*, **627**, L9
- Guenther E. W., Paulson D. B., Cochran W. D., Patience J., Hatzes A. P., Macintosh B., 2005, *A&A*, **442**, 1031
- Hartkopf W. I., Tokovinin A., Mason B. D., 2012, *AJ*, **143**, 42
- Høg E., et al., 2000, *A&A*, **355**, L27
- Hogan E., Jameson R. F., Casewell S. L., Osbourne S. L., Hambly N. C., 2008, *MNRAS*, **388**, 495
- Kalas P., et al., 2008, *Science*, **322**, 1345
- Kato N., Itoh Y., Sato B., 2018, *PASJ*, **70**, 60
- Kervella P., Arenou F., Mignard F., Thévenin F., 2019, *A&A*, **623**, A72
- Kervella P., Arenou F., Thévenin F., 2022, *A&A*, **657**, A7
- King J. R., Villarreal A. R., Soderblom D. R., Gulliver A. F., Adelman S. J., 2003, *AJ*, **125**, 1980
- Kiraga M., 2012, *Acta Astron.*, **62**, 67
- Kuzuhara M., et al., 2022, *arXiv*, **p. arXiv:2205.02729**
- Lafrenière D., et al., 2007, *ApJ*, **670**, 1367
- Lafrenière D., Jayawardhana R., van Kerkwijk M. H., Brandeker A., Janson M., 2014, *ApJ*, **785**, 47
- Lagrange A. M., Desort M., Galland F., Udry S., Mayor M., 2009, *A&A*, **495**, 335
- Langlois M., Vigan A., Moutou C., Sauvage J.-F., Dohlen K., Cos-tille A., Mouillet D., Le Mignant D., 2013, in *Esposito S., Fini L., eds, Proceedings of the Third AO4ELT Conference*. p. 63, [doi:10.12839/AO4ELT3.13317](https://doi.org/10.12839/AO4ELT3.13317)
- Langlois M., et al., 2021, *A&A*, **651**, A71
- Lazzoni C., et al., 2020, *A&A*, **641**, A131
- Leike R. H., Glatzle M., Enßlin T. A., 2020, *A&A*, **639**, A138
- Lodieu N., Boudreault S., Béjar V. J. S., 2014, *MNRAS*, **445**, 3908
- Maire A.-L., et al., 2016, in *Proc. SPIE*. p. 990834 ([arXiv:1609.06681](https://arxiv.org/abs/1609.06681)), [doi:10.1117/12.2233013](https://doi.org/10.1117/12.2233013)
- Maire A. L., et al., 2020, *A&A*, **639**, A47
- Makarov V. V., Kaplan G. H., 2005, *AJ*, **129**, 2420
- Malkov O. Y., Oblak E., Snegireva E. A., Torra J., 2006, *A&A*, **446**, 785
- Marigo P., et al., 2017, *ApJ*, **835**, 77
- Marino S., Yelverton B., Booth M., Faramaz V., Kennedy G. M., Matrà L., Wyatt M. C., 2019, *MNRAS*, **484**, 1257
- Marois C., Correia C., Véran J.-P., Currie T., 2014, in *Exploring the Formation and Evolution of Planetary Systems*. pp 48–49, [doi:10.1017/S1743921313007813](https://doi.org/10.1017/S1743921313007813)
- Martín E. L., Koresko C. D., Kulkarni S. R., Lane B. F., Wizinowich P. L., 2000, *ApJL*, **529**, L37
- Martín E. L., Lodieu N., Pavlenko Y., Béjar V. J. S., 2018, *ApJ*, **856**, 40
- Mesa D., et al., 2021, *MNRAS*, **503**, 1276
- Meshkat T., Kenworthy M. A., Reggiani M., Quanz S. P., Mamajek E. E., Meyer M. R., 2015, *MNRAS*, **453**, 2533
- Messina S., Nardiello D., Desidera S., Baratella M., Benatti S., Biazzo K., D’Orazi V., 2022, *A&A*, **657**, L3
- Michalik D., Lindegren L., Hobbs D., 2015, *A&A*, **574**, A115
- Netopil M., Paunzen E., Maitzen H. M., North P., Hubrig S., 2008, *A&A*, **491**, 545
- Nielsen E. L., Close L. M., 2010, *ApJ*, **717**, 878
- Nielsen E. L., et al., 2019, *AJ*, **158**, 13
- Nielsen E. L., et al., 2020, *AJ*, **159**, 71
- Nordström B., et al., 2004, *A&A*, **418**, 989
- Oelkers R. J., et al., 2018, *AJ*, **155**, 39
- Patience J., Ghez A. M., Reid I. N., Weinberger A. J., Matthews K., 1998, *AJ*, **115**, 1972
- Paulson D. B., Cochran W. D., Hatzes A. P., 2004, *AJ*, **127**, 3579
- Pavlov A., Feldt M., Henning T., 2008, in *Argyle R. W., Bunclark P. S., Lewis J. R., eds, Astronomical Society of the Pacific Conference Series Vol. 394, Astronomical Data Analysis Software and Systems XVII*. p. 581
- Pérez-Garrido A., Lodieu N., Rebolo R., 2017, *A&A*, **599**, A78
- Pérez-Garrido A., Lodieu N., Rebolo R., Chinchilla P., 2018, *A&A*, **620**, A130
- Phillips M. W., et al., 2020, *A&A*, **637**, A38
- Potter D., Martín E. L., Cushing M. C., Baudoz P., Brandner W., Guyon O., Neuhauser R., 2002, *ApJL*, **567**, L133

Pourbaix D., et al., 2004, *A&A*, 424, 727
 Pribulla T., et al., 2014, *MNRAS*, 443, 2815
 Raghavan D., et al., 2010, *ApJS*, 190, 1
 Rameau J., et al., 2013, *A&A*, 553, A60
 Reid I. N., Gizis J. E., 1997, *AJ*, 114, 1992
 Reid I. N., Mahoney S., 2000, *MNRAS*, 316, 827
 Riddle R. L., et al., 2015, *ApJ*, 799, 4
 Robin A. C., et al., 2012, *A&A*, 543, A100
 Saar S. H., Nordstrom B., Andersen J., 1990, *A&A*, 235, 291
 Schneider A. C., Windsor J., Cushing M. C., Kirkpatrick J. D., Shkolnik E. L., 2017, *AJ*, 153, 196
 Sieglar N., Close L. M., Mamajek E. E., Freed M., 2003, *ApJ*, 598, 1265
 Skrutskie M. F., et al., 2006, *AJ*, 131, 1163
 Snellen I. A. G., Brown A. G. A., 2018, *Nature Astronomy*, 2, 883
 Soderblom D. R., Mayor M., 1993, *AJ*, 105, 226
 Soubiran C., et al., 2018, *A&A*, 616, A7
 Squicciarini V., Gratton R., Bonavita M., Mesa D., 2021, *MNRAS*, 507, 1381
 Steiger S., et al., 2021, *AJ*, 162, 44
 Tokovinin A., 2014, *AJ*, 147, 86
 Tokovinin A., Briceño C., 2020, *AJ*, 159, 15
 Tokovinin A., Horch E. P., 2016, *AJ*, 152, 116
 Tokovinin A., Hartung M., Hayward T. L., 2013, *AJ*, 146, 8
 Tokovinin A., Mason B. D., Hartkopf W. I., Mendez R. A., Horch E. P., 2018, *AJ*, 155, 235
 Torres C. A. O., da Silva L., Quast G. R., de la Reza R., Jilinski E., 2000, *AJ*, 120, 1410
 Torres C. A. O., Quast G. R., da Silva L., de La Reza R., Melo C. H. F., Sterzik M., 2006, *A&A*, 460, 695
 Trifonov T., Tal-Or L., Zechmeister M., Kaminski A., Zucker S., Mazeh T., 2020, *A&A*, 636, A74
 Vigan A., Moutou C., Langlois M., Allard F., Boccaletti A., Carillet M., Mouillet D., Smith I., 2010, *MNRAS*, 407, 71
 Vigan A., et al., 2012, *A&A*, 544, A9
 Vigan A., et al., 2017, *A&A*, 603, A3
 Vigan A., et al., 2021, *A&A*, 651, A72
 Wahhaj Z., et al., 2013, *ApJ*, 773, 179
 Wang S., Chen X., 2019, *ApJ*, 877, 116
 White R. J., Gabor J. M., Hillenbrand L. A., 2007, *AJ*, 133, 2524
 Wittenmyer R. A., Marshall J. P., 2015, *AJ*, 149, 86
 Zhang Z., Liu M. C., Best W. M. J., Dupuy T. J., Siverd R. J., 2021, *ApJ*, 911, 7
 Zúñiga-Fernández S., et al., 2021, *A&A*, 645, A30
 Zuckerman B., Song I., 2004, *ARA&A*, 42, 685
 de Zeeuw P. T., Hoogerwerf R., de Bruijne J. H. J., Brown A. G. A., Blaauw A., 1999, *AJ*, 117, 354

APPENDIX A: NOTES ON INDIVIDUAL TARGETS

HIP 15247 F6V star, classified as member of Tuc-Hor in several works (e.g., Zuckerman & Song 2004). It was first spatially resolved into a close pair by Hartkopf et al. (2012). Additional astrometric observations by Tokovinin (2014); Tokovinin & Horch (2016); Tokovinin et al. (2018); Riddle et al. (2015); Galicher et al. (2016b); Meshkat et al. (2015) allows to constrain the binary orbit. The secondary is also detected in *Gaia*EDR3. Significant RV variability (RV rms 6.6 km/s, 3 epochs over 850 days) is reported by Nordström et al. (2004). Single-epoch (Feb 2003) RV by White et al. (2007) (9.1 ± 0.8 km/s) is close to the Nordström et al. (2004) mean value (7.2 km/s). The three determinations by Zúñiga-Fernández et al. (2021) (mean 17.78 ± 0.38 km/s, span 16 days in July-August 2012) are instead off by more than 10 km/s with respect to Nordström et al. (2004) mean value. These variations are larger than the expected ones caused by the known companion, making likely that the system is actually triple. When using BANYAN Σ , the probability of Tuc-Hor membership largely depends on the adopted RV (high when adopting

Nordström et al. (2004) and null for Zúñiga-Fernández et al. (2021) RV). Li EW (White et al. 2007) is more similar to that of Pleiades members, but compatible with Tuc-Hor age considering the dispersion of individual members, while the X-ray luminosity is close to the median value of Tuc-Hor members of similar colors. Considering the uncertainty in the group assignment due to multiplicity, we adopt Tuc-Hor membership, but allowing upper limit to stellar age up to the Pleiades age. For this age, the mass of the secondary results of 0.68 M_{\odot} .

HIP 17439 = HD 23484 Field object with age indicators compatible with an age close to the Hyades. Raghavan et al. (2010) report tentative RV variability but the star results to have roughly constant RV from Nordström et al. (2004) data (rms 0.1 km/s, $N=4$ over 2.8 years), Soubiran et al. (2018) (rms 20 m/s from 5 CORALIE spectra over 13 years), and Wittenmyer & Marshall (2015) (rms 14 m/s from 19 UCLES/AAT spectra over 8 years), with the mean values of the first two of these works in agreement to better than 1 km/s. The star has an extended debris disk, spatially resolved by Herschel (Ertel et al. 2014). Their modelling supports the presence of a two-component disk (belts at 29 and 90 au), possibly with a gap cleared by a massive planet, although a unique very wide belt can not be ruled out. At the expected location of such hypothetical planet (~ 60 -80 au), the $\Delta\mu$ signature (albeit marginally significant) predict a mass of about 6-8 M_{Jup} , which would place it below the observed detection limits for our images. RV data do not provide significant constraints at such wide separations. The disk is not revealed in scattered light in our SPHERE images.

HD 28736 = HIP 21152 Member of Hyades from several works in the literature and confirmed with BANYAN Σ analysis with updated kinematic parameters. A new brown dwarf companion is detected in this study, as discussed in Sec. 4.5.

HD 28992 = HIP 21152 = TYC 1266-278-1 Member of Hyades from several works in the literature and confirmed with BANYAN Σ analysis with updated kinematic parameters. RV monitoring from Paulson et al. (2004) (rms 21 m/s, 11 measurements, baseline 5.2 yr with HIRES/Keck) and Soubiran et al. (2018) (rms 39 m/s, 11 measurements, baseline 2.8 yr with SOPHIE/OHP) rule out massive companions at moderately close separation. The absolute RV by Nordström et al. (2004) agrees within error with the recent ones by Soubiran et al. (2018) and *Gaia* Collaboration et al. (2018).

HIP 22506 = HD 31026 = TYC 7589-1186-1 Li EW (Torres et al. 2006), rotation period (Kiraga 2012), and X-ray emission are marginally compatible with the distributions of Pleiades (125 Myr) and Argus (50 Myr) members, but intermediate between the mean loci of these groups. There are clear indications of RV variability (peak-to-valley 17 km/s) from sparse RV determinations available in the literature (Nordström et al. 2004; Torres et al. 2006; *Gaia* Collaboration et al. 2018). The assignment to known groups depends on the adopted RV. We obtain high membership probability for Argus when adopting *Gaia*RV or without RV, and poor match for Nordström et al. (2004); Torres et al. (2006) RV. The expected RV to optimize the Argus membership is very close to the mean values of the three determinations. We then adopt the Argus with upper limit at Pleiades age 50^{+75}_{-10} Myr. Our SPHERE images do not reveal any candidate. It is possible that the $\Delta\mu$ signature is due to the unseen spectroscopic companion.

GJ 3346 = HIP 24874 = HD 34865 = TYC 5902-586-1

Star with white dwarf companion, discovered and characterized as part of the present project. Previously published in Bonavita et al.

(2020). It was included in the sample as it appears as a young star with moderately high activity level, due to accretion of material lost by the WD progenitor.

HIP 27441 = HD 39126 = TYC 7601-371-1 Field object. Age indicators consistently provide an age of 250 ± 100 Myr. The star has a wide common proper motion companion, 2MASS J05483951-3956087, at 34" (1400 au at the distance of the star). From colors and absolute magnitudes, the companion is expected to be a M2 star.

HIP 28474 = HD 41071 = RT Pic The star is classified as member of Columba association in several works and membership is confirmed by our analysis with updated *Gaia* inputs. Age indicators support a young age although Li EW and rotation period are in mild disagreement with the typical values of Tuc-Hor and Columba members and more similar to Pleiades and AB Dor ones. For this reason, we adopt Columba age but with upper limit at the age of the Pleiades. The classification as eclipsing binary with 2.6 mag deep eclipses (Malkov et al. 2006) appears spurious, as there are no indications of them in the TESS light curve (4 sectors) and the RV results constant over decades at km/s level (Nordström et al. 2004; Gaia Collaboration et al. 2018) and at few tens of m/s level over three months from HARPS data. A close stellar companion was identified by Chauvin et al. (2010) and further observed by Tokovinin & Briceño (2020). It is also detected in our data (mass from photometry 0.16 Msun) and is the responsible of the $\Delta\mu$ signature.

HIP 29724 = HD 43976 Young field object, not associated to any known moving group. Li EW and X ray emission are close to the mean locus of the Pleiades while the rotation period from TESS suggests a slightly older age. A new substellar companion is detected in this study (see Sec. 4.6 for details).

HIP 33690 = HD 53143 Star with resolved debris disk (Kalas et al. 2008). The star is flagged as a possible member of IC2391/Argus in some literature works (e.g., Nielsen et al. 2019). However, BANYAN analysis with updated *Gaia* parameters return 0% membership probability for this group and no significant probability for other known MGs. Furthermore, the non detection of Lithium (Torres et al. 2000) clearly rules out the young age of IC2391/Argus. The Li non-detection and the other age indicators are fully compatible with an age similar to the Hyades. The companion candidate seen in our images and previously identified by Wahhaj et al. (2013) is a background object.

HD 57852 = HIP 35564 = HR 2813 = TYC 8132-2112-1 Bona-fide member of Carina-Near MG, confirmed with BANYAN Σ analysis using the updated kinematic parameters. The star has highly significant RV variability (Andersen & Nordstrom 1983; Pribulla et al. 2014; Desidera et al. 2015; Gaia Collaboration et al. 2018), although without orbital solution. Peak-to-valley RV range for the available data is 13 km/s. The longest-period plausible orbital solution consistent with the data yields a period of 994 d with moderately high eccentricity. Shorter periods are also possible considering the poor time sampling. The spectroscopic component is likely the responsible of the $\Delta\mu$ signature and of the large RUWE in *Gaia*EDR3 (8.69), and it is expected to be at a separation too close to the star to be detected in SPHERE images. HD 57852 has a wide companion (HD 57853) at 9", which is itself a spectroscopic binary with three components with total mass 2.4 Msun (Saar et al. 1990; Desidera et al. 2006). The system is then a hierarchical quintuple. The source detected at 4.9" and previously identified by Chauvin et al. (2015) is a background object.

n Pup A = HD 60584 = TYC 6539-3802-1 Mid-F type star with a

nearly twin wide companion (n Pup B = HD 60585 at 9.9"). Katoh et al. (2018) found the primary to an SB1 with period 366 days, eccentricity 0.49, RV semi-amplitude 12 km/s, corresponding to a minimum mass of 0.5 Msun. This orbital solution and variability above 1.6 km/s (peak-to-valley) are not supported by HARPS RV (Lagrange et al. 2009; Trifonov et al. 2020). The HARPS RV variability appears to be dominated by short-term variations (intra-night and from contiguous nights) with limited variability on longer timescales. The star is an X-ray source, but considering the very limited age dependence of X-ray emission for mid-F stars we rely only on isochrone fitting for our age estimate. The identification of a faint BD candidate, compatible with the $\Delta\mu$ signature, is discussed in Sect. 4.7. The source at 4.4" is a background object.

HIP 48341 = HD 85364 = HR 3899 = 6 Sex = TYC 4899-1904-1 Early type star, identified as a possible member of UMa group by Soderblom & Mayor (1993); King et al. (2003). Chupina et al. (2006) classified it as a member of corona surrounding the UMa nucleus. Kinematic analysis using BANYAN returns a field object classification. Independently on the kinematic assignment, isochrone fitting yields an age of 660 ± 260 , formally compatible with Ursa Major. The star has also IR excess indicating the presence of a debris disk (Chen et al. 2014).

HIP 52462 = HD 92945 = V419 Hya Star with spatially resolved debris disk (Golimowski et al. 2011; Marino et al. 2019). The stellar properties and the presence of companions combining imaging, RV, and astrometric signatures were recently investigated by Mesa et al. (2021).

HIP 59726 = HD 106489 Field object with age similar to the Hyades. The RV results constant within 0.5 km/s from few literature measurements spanning several decades.

HIP 61804 Young star, not associated to any known moving group. The rotation period from TESS and chromospheric activity are similar to Pleiades members.

HIP 63734 = HD 113414 F7/F8 star, investigated by Nardiello et al., submitted as a candidate comoving object to TOI-1807 and TOI-2048, 300 Myr old stars both hosting transiting planets. The star results likely younger, with an estimated age of 150 Myr from Li EW and X-ray emission. The identification of a faint BD candidate, compatible with the $\Delta\mu$ signature, is discussed in Sect. 4.7.

HIP 63862 = HD 113553 = TYC 8258-871-1 BANYAN Σ yields a 53% membership probability for Carina-Near MG. The star was not considered a candidate members in past studies. With a field star classification and a variety of age indicators, Vigan et al. (2017) estimated an age of 180 Myr with 120-250 limits, fully consistent with the age of Carina-Near MG. We adopt Carina-Near MG age, with expanded age limits from indirect age indicators due to the moderately low membership probability. Mean RVs from Nordström et al. (2004); Torres et al. (2006); Gaia Collaboration et al. (2018) agree very well, while Nordström et al. (2004) mentioned a marginally significant variability (rms 0.5 km/s, 11% probability of constant RV). The source at 4.4", previously detected by Chauvin et al. (2015), is a background object.

HIP 71899 = HD 129501 = TYC 1483-1030-1 F8 star. A bright source is detected within IRDIS field of view and is also seen (without full astrometric solution) in *Gaia* Collaboration et al. (2018, 2021). The combination of SPHERE and *Gaia* data confirms its physical association, with a mass of 0.39 Msun. Indications of the young age of the system comes from the prominent X-ray emission (intermediate

between Hyades and Pleiades of similar color) and rotation period from KELT (Oelkers et al. 2018), comparable to Pleiades stars although with the limited age sensitivity expected for F type stars. Isochrone fitting, when adopting solar metallicity is compatible with the young age from activity and with a broader range up to 3 Gyr. The sub-solar metallicity by Stromgren photometry (Casagrande et al. 2011) (which however could be biased by stellar activity) would instead indicate an evolved star. Finally the kinematics is slightly outside the kinematic space of young stars. The limited amount of data (no light curve from TESS, no high resolution spectra available in public archives) and the impact of binarity prevents a better age determination. Therefore, we adopt the X-ray age, keeping as upper limit the results of isochrone fitting.

HD 143600 = HIP 78549 The star is a well known recognized member of Upper Sco association (e.g., de Zeeuw et al. 1999) and membership is confirmed by our own check with *Gaiadata*. The star was discovered to be a close visual binary (sep 0.325", $\Delta K_s=3.99$) by Lafrenière et al. (2014). There is no significant IR excess, while the star has a significant reddening ($E(B-V) = 0.14$) from comparison of observed and expected colors for the B9.5 spectral type.

HIP 108912 All the indicators are consistent with an age intermediate between Hyades and Pleiades, and similar to Group X. RV by Nordström et al. (2004); *Gaia* Collaboration et al. (2018) are in agreement within errors.

HIP 112491 Field object; age indicators consistently suggest an age close to that of the Hyades.

HIP 112581 Field object with age similar to the Hyades. A close candidate (estimated mass 0.14 M_{\odot} from photometry) is identified at 0.7", very likely a true companion considering the small projected separation and the presence of the astrometric signature, roughly compatible with the properties of the observed candidate.

TYC 9339-2158-1 Wide visual binary, with the primary of the system, the G1 star HIP 116063 = HD 221231 being at 36". The analysis of the age indicators yields to an age intermediate between Hyades and Pleiades (Vigan et al. 2017).

HIP 116768 Am star. Isochrone fitting (using the T_{eff} calibration by Netopil et al. 2008) indicate that the star is somewhat evolved outside main sequence. However, the star is likely a binary ($\text{RUWE}=6.3$ in *Gaia*EDR3) so parallax (which has a large error), magnitude, and age can be biased by binarity. The star has a low membership probability in Argus (29.8%), in contrast with the isochrone age.

ACKNOWLEDGEMENTS

This research has made use of the SIMBAD database and of the VizieR catalogue access tool operated at CDS, Strasbourg, France, and of the Washington Double Star Catalogue maintained at the U.S. Naval Observatory. This work has made use of data from the European Space Agency (ESA) mission *Gaia* (<http://www.cosmos.esa.int/gaia>), processed by the *Gaia* Data Processing and Analysis Consortium (DPAC, <http://www.cosmos.esa.int/web/gaia/dpac/consortium>). Funding for the DPAC has been provided by national institutions, in particular the institutions participating in the *Gaia* Multilateral Agreement. This work has made use of the SPHERE Data Centre, jointly operated by OSUG/IPAG (Grenoble), PYTHEAS/LAM/CeSAM (Marseille), OCA/Lagrange (Nice), Observatoire de Paris/LESIA (Paris), and Observatoire de Lyon/CRAL, and supported by a grant from Labex OSUG@2020

(Investissements d’avenir – ANR10 LABX56). CF acknowledges support from the Center for Space and Habitability (CSH). This work has been carried out within the framework of the NCCR PlanetS supported by the Swiss National Science Foundation. This work has been supported by the PRIN-INAF 2019 "Planetary systems at young ages (PLATEA)" and ASI-INAF agreement n.2018-16-HH.0. KM acknowledges funding by the Science and Technology Foundation of Portugal (FCT), grants No. IF/00194/2015, PTDC/FIS-AST/28731/2017, and UIDB/00099/2020. For the purpose of open access, the authors have applied a Creative Commons Attribution (CC BY) licence to any Author Accepted Manuscript version arising from this submission.